Per-/Poly-fluoroalkyl Substances (PFASs) Treatment and Mechanistic Insights: Photo-catalyst and Photo-Electro-catalyst Materials Application

Yaswanth K. Penke,[a*] Kamal K. Kar [a,e]

[a] Department of Mechanical Engineering Indian Institute of Technology Kanpur, Kanpur, Uttar Pradesh, 208016, India

[b] Advanced Nanoengineering Materials Laboratory, Materials Science Programme, Indian Institute of Technology Kanpur, Kanpur, Uttar Pradesh, 208016, India

*** Corresponding author**

yaswanth.mighty@gmail.com

Keywords: *PFASs; Environmental Remediation; Degradation; Heterogeneous catalysis; Mechanistic Pathways.*

Abstract

The PFASs contamination (Per-/Poly-fluoroalkyl Substances ~ 4000 compounds) is influencing the humane through soil and aquifers contamination, resulting in the endocrine-disrupting symptoms (EDS). PFASs decontamination involves both (i) Capture/non-degradation techniques and (ii) Degradation techniques. In the present work, a detailed discussion on various photo-catalytic/electrocatalytic electrode materials (Fe/Ti/Zn/Bi/C etc.) over PFASs degradation is provided. The authors have focused onto the recent literature published in the last couple of years for citing research outputs and schematic figures. The analysis of both radical species (e.g., hydroxyl/sulphate species) and direct electron transfer (DET) mechanisms are given. An insightful discussion of the impact on various degradation mechanisms (decarboxylation, and hydrodefluorination) onto various PFASs has been provided. A different set of examples are provided in describing both electron (e-) based oxidation and hole (h+) based oxidation phenomenon. The state-of-the-art novel inventions towards pilot-scale studies and field-level applications are discussed with explaining the possible limitations (e.g., light source etc.). The factors influencing the degradation process (i.e., Electrode potential, Current density, Impact of dosage, pH, Radical species, Competing ions, Temperature and light source) are also detailed prior to the future perspective and conclusions.

Table of Contents

1. **Introduction**
2. **Photo-catalytic/electrocatalytic electrodes**
    - 2.1 Ti-based
    - 2.2 Fe-based
    - 2.3 Bi-based
    - 2.4 Zn- based
    - 2.5 Other metal systems
    - 2.6 Carbon structures
3. **Degradation Mechanism and Pathways**
    - 3.1 Electron (e^-) based oxidation
    - 3.2 Hole (h^+) based oxidation
4. **Pilot studies and Field level Applications**
5. **Influencing Parameters over Degradation**
    - 5.1 Electrode potential, Current and Composition
    - 5.2 Impact of dosage (catalyst)
    - 5.3 Effect of pH
    - 5.4 Radical species activity
    - 5.5 Effect of Temperature and light source
    - 5.6 Effect of organic matter and other competing ions
6. **Future Perspectives and Conclusions**
7. **References**

1. Introduction

Persistent organic pollutants (POPs) are toxic organic chemicals that adversely affect both human health and the environmental systems [1–5]. They can transit through the air and water across the boundaries due to their nature of persistence. POPs are lipophilic chemicals with extended half-lives, leading to bioaccumulation in the food chain [6,7]. POPs are classified into various artificially produced chemical compounds like polychlorinated biphenyls (PCBs), dioxins, perfluorinated compounds (PFCs), organochlorine pesticides (OC), and polyaromatic hydrocarbons (PAHs). Per- and polyfluoroalkyl substances (PFASs) are a class of aliphatic organofluorine compounds in which the hydrogens are either partially or fully substituted by a fluorine [8–10]. PFASs are characterized by a hydrophobic fluorinated carbon chain bound to a functional group head of hydrophilic nature (e.g., carboxylic or sulphonic acids). The majority of PFASs exist in anionic form due to strong acidic functional groups; even the cationic and zwitterionic PFASs also exist. The hydrophilic head group of the PFASs result in high solubility in aqueous systems resulting in high mobility. The PFASs are distinguished as long-chain and short-chain, depending on the number of carbon groups. The polar covalent bond between the carbon and fluorine of the PFAS compounds is the stronger resulting in the extremely high thermal and chemical stability of these molecules [11–17]. These persistent organic contaminants possess unique properties such as chemical/thermal stability and a hydrophilic-lipophilic nature, all of which are desirable for various commercial applications (e.g., stain repellents, fire-fighting foams, non-stick cookware, and food contact papers) as shown in **Figure 1** [18,19]. The intensive production of these PFAS substances began around the early 40's (i.e., 1940). In recent years the fate, transport, and non-reactive characteristics of many kinds of PFASs resulted in ubiquitous occurrence in contaminating aqueous (surface, underground) and soil environments in the larger context, which has drawn the greater attention of the scientific community [20–25]. Exposure to PFASs contaminated drinking water has been

linked to various ailments resulting in cancers (kidney and testicular), ulcerative colitis, pregnancy/fertility problems, liver issues, thyroid disorder, and high cholesterol.

The general remediation processes of PFASs involve a couple of mechanisms i) Capture/non-degradation techniques (adsorption, coagulation, membrane filtration, Ion-exchange ozofractionation, etc.) [11,26–30], and ii) Degradation techniques (catalysis, sonochemical, advanced oxidation/reduction processes, electrochemical oxidation, photocatalysis, thermal/plasma-degradation, bio-degradation, etc.) [31–41]. Both the non-degradation and degradation technologies are of equal concern and, in general, are being discussed in a combined manner to address the efficacious and economical treatment technologies for PFAS remediation on different platforms [42–47].

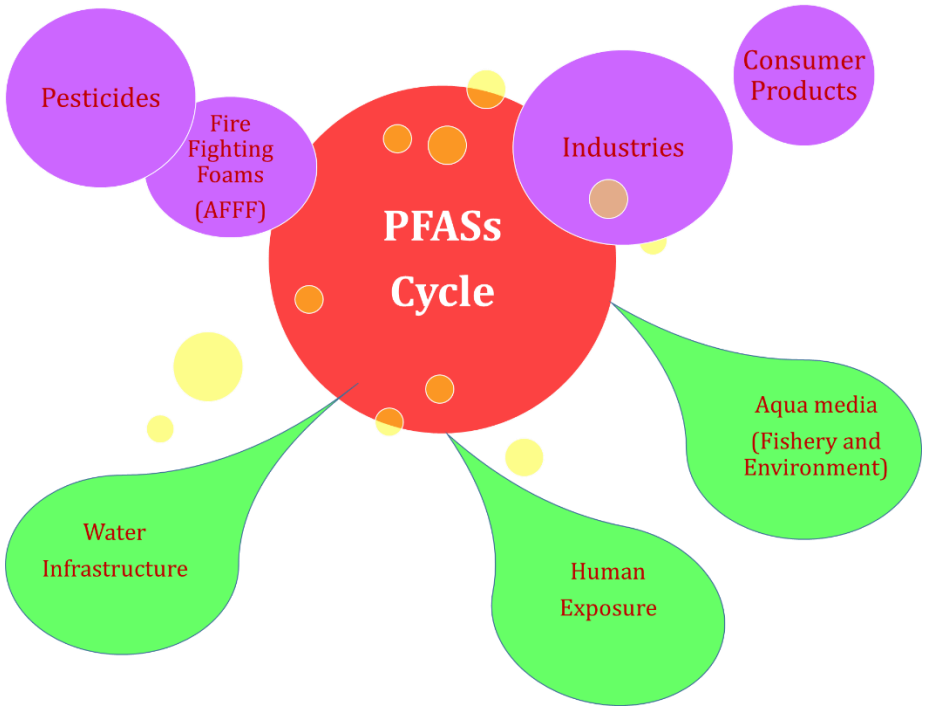

Figure. 1. PFAS cycle illustrating their ubiquitous presence.

The structural aspects of various PFASs (e.g., PFOA, PFOS) and the recent substitute compounds (e.g., Gen X) are observed in **Figure 2**. Novel nanotechnologies show significant potential for PFAS remediation. The synergistic approach of physical adsorption and photochemical reactions (UV band: 180 - 360 nm) onto these engineered nano-materials (e.g., TiO_2, Fe_2O_3, Ga_2O_3, In_2O_3, and CeO_2, etc.) demonstrated great ability in removing PFASs from aqueous solutions [43]. In addition to simple adsorption, the involvement of radical species through various heterogeneous catalytic processes towards multi-synergistic based PFASs remediation has also assisted the decontamination aspects [48]. The decomposition reaction of PFASs (e.g., PFCA) is initiated by a Kolbe decarboxylation in an electron acceptor forming perfluoroalkyl radicals. Photogenerated holes and hydroxyl radicals are the primary electron acceptors in the photocatalytic degradation system [49,50]. During the photocatalysis process, the photogenerated holes on the surface of the photocatalyst rapidly generated hydroxyl radicals in water. A few metal oxides (e.g., In_2O_3) outperformed other materials in terms of decomposition, and defluorination ratios with less energy consumption, in the same time parameter.

A recent analysis of PFAS exposure impact in Europe and the United States identified annual direct healthcare expenditures at € 52−84 billion and $ 37−59 billion, respectively [51]. These costs will not be taken care of by the polluter (or) the contaminant source and should be the responsibility of the citizens, health care/welfare units, and the taxpayers. As per the new European drinking water guidelines the maximum limit value for sum concentration of 20 PFASs (i.e., PFBA, PFPeA, PFHxA, PFHpA, PFOA, PFNA, PFDA, PFUnDA, PFDoDA, PFTrDA, PFBS, PFHxS, PFHpS, PFOS, PFNS, PFDS etc.) is 0.1 μg/L (0.1 ppb) [52]. The US Environmental Protection Agency (USEPA) health advisory level of individually or combined PFASs is 70 ng/L (0.07 ppb). Hence a new class of metal-based nano-adsorbents/heterogeneous catalysts with a better redox activity, photocatalytic nature in the

visible band (400-700 nm), and economically feasible materials (e.g., Fe, Mn, Al) need to be studied as near-futuristic research and innovation technologies.

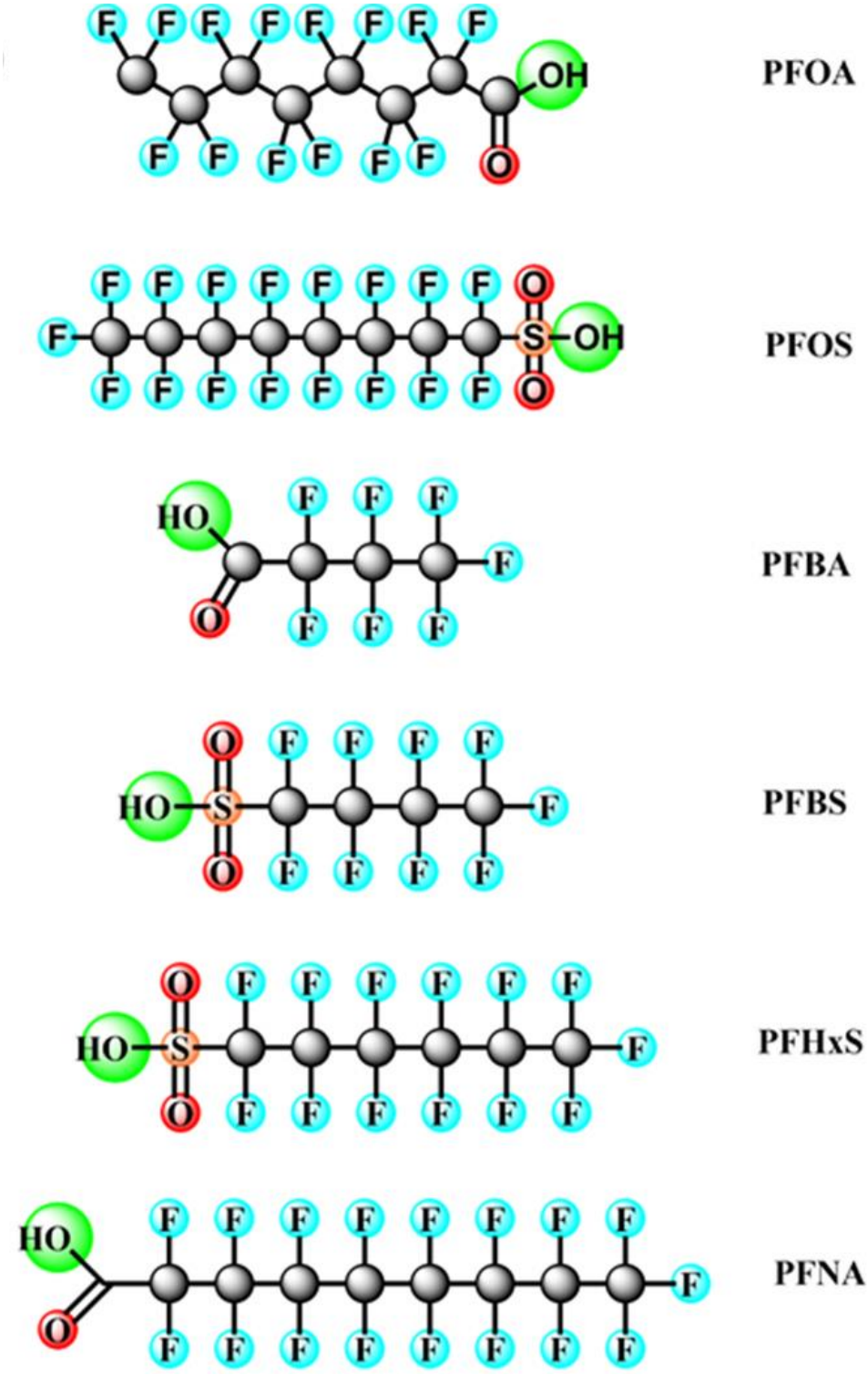

Figure. 2. Chemical structure of PFOA, PFOS, PFBA, PFBS, PFHxS, PFNA [18] (Copyright Elsevier).

Recently, a few research groups developed a new approach of metal ion activated external oxidants (Peroxymonosulfate: PMS, Persulfate: PS) in generating reactive radical species (i.e., sulfate radicals) for remediating various organic contaminants (e.g., estrogenic compounds) [53,54]. A recent article on reviewing the light-induced advanced oxidation processes (AOPs) as PFAS remediation methods are detailed elsewhere [32], whereas the present work focuses on light-induced, electrochemical supported [electro-oxidation] AOPs in addition to the electro-kinetic/coagulation-sorption. The analysis and the sensing part, in addition to the modeling aspects of these emerging contaminants, are also receiving more extensive attention from the peers considering the global concern [55–59].

2. Catalytic and Electrochemical Degradation Treatment

In recent years, the catalytic processes have shown a significant impact on the degradation of various PFASs through different modes of operation like Advanced Oxidation Processes (AOPs) by generating strong oxidation species (e.g., reactive oxygen species (ROS), reactive sulphur species (RSS)). Various photochemical AOPs through photocatalysts like Fe-TiO_2, TiO_2– rGO, Pb-$BiFeO_3$, and Ti_3C_2 (MXenes)/TiO_2 was observed with significant degradation efficiencies [60]. A brief discussion on various catalytic/electrode materials for photocatalytic and electro-oxidation are discussed below.

2.1 TiO_2 based electrodes

In a recent study, the electro-oxidation process was provided with individual and simultaneous degradation reactions towards PFOA and GenX using a titanium suboxide (TSO) reactive membrane anode [61]. The anode plays a vital role in the electro-oxidation process, whereas the cathode is crucial in the electro-reduction process. The PFOA degradation values were observed up to 73.9 ± 3.5% and 19.9 ± 5.0% at current densities of 8 mA cm^{-2} and 1 mA cm^{-2}, respectively (t ~ 180 min). The degradation process can be identified qualitatively by analyzing

the chemical oxygen demand (COD) in permeate and retentate. A decreased COD in the retentate over time confirms the degradation. Even the flux densities could also influence the degradation kinetics due to the formation of oxygen bubbles near the anode surface. These bubbles adsorb the PFOA species due to the hydrophobic nature, eventually hindering the anode exposure resulting in low decomposition. Titanium suboxides (TSO) were also verified for the electro-oxidation (EO) based degradation of PFOS using Ti_4O_7 and Ti_9O_{17}, where the former exhibited better efficiency due to a more significant fraction of Ti^{3+} (**Figure 3**) [62]. Complete degradation of PFOS ($C_i \sim 2$ μM) was observed for 20 min under the current density of 60 mA cm^{-2} onto both nano-Ti_4O_7 and micro-Ti_4O_7 anodes. The formation of a strong signal at 689.5 eV in the XPS (X-ray photoelectron spectroscopy) confirmed the near-surface occurrence of fluoride atoms through the Ti-F bond. A significant amount of fluorine has been released into the aqueous systems during the electro-oxidation process (40-99 % in 4 - 14 h). A better effective electro-active surface area (EESA) of nano Ti_4O_7 anode has resulted in better electro-oxidation performance than other similar anodes (e.g., Boron Doped Diamond: BDD). The pore structure of the sintered individual anodes has shown a high impact on the reaction parameters. The pores with smaller dimensions (< 1.03 μm) resulted in restrictive electrolyte transport, diminishing the effective electro-active surface. The Reactive Electrochemical Membrane (REM) module has shown better adsorption to the batch reactor systems due to the availability of inner pore surfaces for PFOS adsorption during the REM module, considering the availability of more electrode surfaces, better activation by direct electron transfer, and efficient interphase mass transfer (i.e., convention facilitated dispersion). Diffusion and adsorption characteristics were better observed in the micro anode module due to the pores in the 2 - 4 nm dimension to the nano anodes (PFOS molecular length: 1.32 nm). 3D SG (Sulfonated Graphene)-TiO_2-QD aerogels were reported for PFOA's high ability, which derived from fast adsorption and effective photocatalytic decomposition [63]. Sodium dodecyl

sulfate (SDS) has been used as a surfactant to connect the hydrophilic ($TiCl_3$) and the hydrophobic (SG sheets) surfaces. The hydrophobic surface and increased valence band position of 3D SG- TiO_2 QD aerogels enhanced the interaction with PFOA and the capability of holes to trap electrons facilitating to yield more h^+ for attacking the adsorbed PFOA. 3D SG-TiO_2 QDa (2.5 nm) owned the fastest kinetics K_{app} (1.898 E^{-4}/s), compared to 3D SG-TiO_2 QDb (3 nm; 1.530 E^{-4}/s) and 3D SG-TiO_2 NP (48 nm; 9.283 E^{-5}/s) systems conforming the smaller size of TiO_2 enhanced the photocatalytic parameters towards degradation.

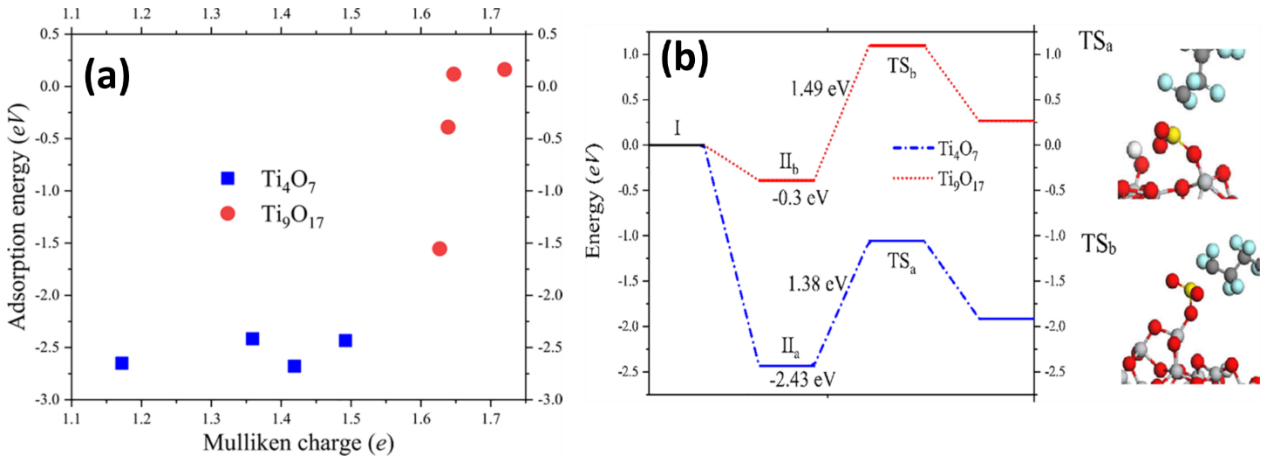

Figure 3. (a) Correlation between the Mulliken charge of Ti atom and the adsorption energy of PFOS on Ti_9O_{17} and Ti_4O_7 cluster. (b) The energetics of PFOS interaction with Ti_4O_7 and Ti_9O_{17} clusters. IIa and IIb corresponds to the states of PFOS adsorbed on Ti_4O_7 and Ti_9O_{17} cluster, respectively; TSa and TSb are the transition states of PFOS degradation on Ti_4O_7 and Ti_9O_{17} cluster, respectively. Color definition: Dark Gray: Carbon; Cyan: Fluorine; Yellow: Sulfur; Red: Oxygen; Light Gray: Titanium; White: Hydrogen. (For interpretation of the references to color in this figure legend, the reader is referred to the web version of this article.) [62] (Copyright Elsevier)..

In another study, simple TiO_2 could not degrade PFOA efficiently (~ 10 %), and only 2% of defluorination was observed. Whereas with TiO_2-rGO, the degradation efficiencies have risen to 86 %, corresponding to the defluorination and mineralization values of 30 and 43 %,

respectively [64]. The main advantage of rGO is reducing the recombination of the charge carriers and band-gap tuning. A graphene oxide – TiO_2 anode coated FTO glass has been verified for PFOA degradation with a comparative study between electrochemical (EC) and photo-electrochemical (PEC) modules [65]. An impressive degradation efficiency (100 %) was observed for 0.5 mg/L PFOA aliquot at pH of 5.2 and 16.7 mA cm^{-2} density in 4h. The possible degradation has occurred through four different pathways: decarboxylation followed by oxidation, defluorination, hydroxylation, and Cl-F replacement. Other carbon structures like activated carbon (AC) associated with titanium and iron constituents have been reported for PFOA degradation. A novel, calcined Fe/TNTs@AC (550 ^{O}C) photocatalyst provided up to 90% of PFOA degradation after 4 h under UV irradiation (~ 254 nm) and 62 % conversion into fluoride ions (F^{-}) [66]. The degradation parameters of PFOA are around 23.8 %, 68.7 %, and 83.3 % for TNTs@AC, non-calcined Fe/TNTs@AC, and calcined TNTs@AC, respectively. Defluorination (i.e., realize of F^{-} ions) values of Fe/TNTs@AC were 1.5, 2, and 4 times higher than TNTs@AC, non-calcined Fe/TNTs@AC, and non-calcined TNTs@AC, respectively. Fe/TNTs@AC offers some unique advantages like better adsorption followed by focused photo-irradiation onto the PFOA-laden solid rather than bulk water sample. Increasing Fe content (> 1 %) resulted in suppressing the degradation values as recombination centres for the photogenerated electrons and holes due to the quantum tunneling effects. Efficient photo-degradation in the present hybrid (Fe, Ti, and AC) is due to carbon nanoparticles facilitating hydrophobic and anion-π interactions, damped electron-hole recombination due to carbon coating/Fe centres, better surface charge potential due to Fe(III) presence, and radicals generation (• OH) by Fe(III)-Fe(III) redox reaction cycle. The major advantage of Fe_2O_3 with TiO_2 would narrow the bandgap (2.1 – 2.3 eV for Fe_2O_3; 3.0 – 3.2 eV for TiO_2) of the hybrid/composite to enhance the performance in the visible band.

2.2 Fe based electrodes

The interaction of nano-ferrites ($Zn_xCu_{1-x}Fe_2O_4$) with PFOA under UV light irradiation was understood with the generation of photoactive species like oxalate radicals $[C_2O_4]^-$ which are further transformed into carbon-cantered radicals $CO_2^{\bullet-}$ and carbon dioxide [67]. The metal oxide catalyst likely enhanced the photo-production of hydroxyl radical species (•OH) due to the synergism of Zn and Cu centres. The optimal degradation conditions were observed at 0.1 M of oxalic acid, pH of 1.73, and 8.3 mg/ml of $Zn_{0.5}Cu_{0.5}Fe_2O_4$ under 450 W (UV light source). The presence of multiple oxidation centres (Fe^{2+}/Fe^{3+}) and redox reactions among individual centres (i.e., $Fe^{2+} \leftrightarrow Fe^{3+}$) benefited the formation of sulphur radical species ($SO_4^{\bullet-}/S_2O_8^{\bullet-}$) influencing the degradation parameters [68]. Iron-activated persulfate oxidation (IAPO) is one of the most advanced in-situ remediation techniques, which has recently been reported with approximately 64 % degradation efficiency for PFOA under illuminated anoxic conditions (t ~ 4 h, T ~ ambient) [68]. The degradation magnitudes are about seven times (7X) higher in anoxic conditions relative to the oxic conditioned experiments and five times (5X) better reduction during illumination over dark conditions (both anoxic). Fe-doped zeolites have reported molecular oxygen as the terminal oxidant with > 99 % photochemical degradation (UVA) of PFOA (t ~ 24) in slightly acidic conditions (pH ≤ 5 .5) [69]. The hydrophobic forces provided by the zeolite channels for the perfluoroalkyl chains play a major role in the iron-catalyzed photo-degradation process. Higher pH values show a negative effect on photochemical degradation due to a lower fraction of PFOA-Fe^{3+} complexes favouring non-specifically adsorbed species caused by ligand exchange (i.e., Fe-H_2O by Fe-OH^-). Fe(III)-loaded zeolites in ambient conditions with oxygen (O_2) as the terminal oxidant are reported with efficient PFOS degradation performance (~ 99 % in 96 h) with 254 nm ultraviolet (UV) light [70].

In a competing ion study, except for sulphate (SO_4^{2-}), other anions such as Cl^-, NO_3^-, and ClO_4^- showed negligible impact on the degradation. This trend was attributed to the activity of SO_4^{2-} to coordinate with ferric ions. Iron-porphyrin loaded camphor leaf biochar [Fe(TPFPP)/BC] were used in the presence of ascorbic acid, and persulfate (PS), showing a PFOA degradation efficiencies of 56.8, 75.9, 90.9 % in 5 min, 30 min, and 12 h [71]. A significant rise in the degradation efficiency was observed with increased PS concentration (0 – 60 mM), whereas the catalyst dose has shown better influence up to 1 g/L loading. Acidic pH values influenced the removal parameters (90.7 % at pH 2), which may be due to $SO_4^{-\bullet}$ could be formed by H^+ catalysis, whereas radicals were depleted in alkaline conditions. The utilization of ascorbic acid acted as an electronic circulation agent, which promoted the transfer of electrons to BC to regenerate the consumed radicals, which assisted the electron transfer process in Fe(TPFPP)/BC. Zero-valent iron (ZVI) alone and a mixture of ZVI and biochar (ZVI + BC) for PFOA and PFOS degradation were observed with 60 and 94% of input removal (C ~ 18,500 μgL^{-1}) [72]. The PFASs removal mechanisms for ZVI systems are observed likely through sorption, reductive defluorination, and H-bonding. Unknown intermediate degradation products such as $C_6F_{13}CFHCOOH$, $C_6F_{13}CH_2COOH$, $C_7F_{15}CFHSO_3H$, and $C_7F_{15}CH_2SO_3H$ might get included with PFOA and PFOS defluorination products. Iron-clay- cyclodextrin polymer composite (Fe-MMT-βCD-DFB) observed with an efficient oxidation and better degradation towards both PFOA (80 %) and PFOS (73 %), with corresponding defluorination efficiencies around 73.2% and 73.5%. An adsorptive photocatalyst consisting of iron (hydr) oxides (ferri-hydrite-Fh and hematite- Ht) and carbon spheres (FeO/CS) was reported with 95.2% photodegradation and 57.2% defluorination of pre-concentrated PFOA in 4 h. The smaller energy gap between the HOMO and valence band or LUMO and conduction band for Fh predicts a more favorable charge transfer from PFAS species to Fh than Ht, accounting for better photocatalytic activity of Fh (**Figure 4**).

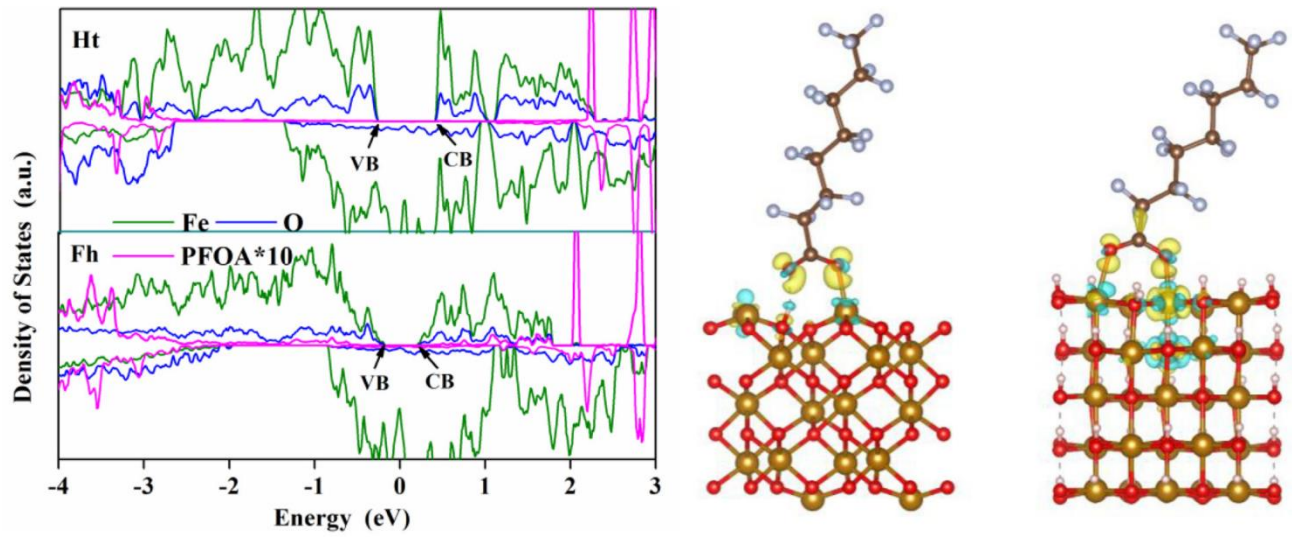

Figure 4. (a) Density of states of PFOA-adsorbed hematite and ferrihydrite (For visual clarity, the data of PFOA is scaled up by a factor of 10). Charge density difference of the PFOA-adsorbed hematite (b) and PFOA-adsorbed ferrihydrite (c). The yellow and blue iso-surfaces represent charge accumulation and depletion in the space, respectively. [73] (Copyright Elsevier).

2.3 Bi based electrodes

Hydrothermal prepared single-crystalline BiOCl nanosheets have been verified for the PFOA degradation through photocatalytic degradation, where {010} facets have shown 2.64 folds better rate constants to {001} facets [74]. The synergistic occurrence of radical species (•OH), photogenerated holes, and better positive charge parameters have influenced the impressive rate parameters of the {010} surface. Better degradation abilities are observed in the acidic conditions due to the more positively charged BiOCl facets resulting in the efficient electrostatic attraction of anions (i.e., $C_7F_{15}COO^-$). In comparison, a simple chemical precipitation method by adding Ca^{2+} (2 mM) has improved the removal process efficacy by 3.3 and 4.3-fold, for {001}-BiOCl and {010}-BiOCl facets, respectively. Bromine doped BiOI ($BiOI_{0.95}Br_{0.05}$) was provided high photocatalytic activity under UV irradiation over (001) facet

towards 96 % decomposition and 65 % mineralization of PFOA within 120 min and 180 min, respectively [75]. Novel BiOI@Bi_5O_7I p-n heterojunction photocatalysts were observed for PFOA degradation efficiency of 30 – 82 % under solar light irradiation [76]. The corresponding physico-chemical parameters of the catalyst calcinated at different temperatures (350 – 450 ^{O}C) influenced the degradation parameters, whereas the sample at 390 ^{O}C showed better abilities due to uniform morphology. Higher pH values (pH > 4.5) and larger initial concentrations of PFOA (> 5 mg/L) have shown a diminishing effect on the degradation parameters. BiOCl/rGO nano-composites integrated from photocatalysis, ozonation, and electrocatalysis have shown 95.4% degradation of PFOA (t ~ 3h) with UV irradiation (254 nm) [77]. Whereas the removal efficiencies in the individual and hybrid processes (t ~ 3h) are observed around 2.2 % (UV irradiation), 4.0 % (EC: electro-catalysis), 9.0 % (ozonation), 30.1 % (PC: photocatalysis), 80.5 % (PC/O_3), and 56.1 % (PEP: photoelectroperoxone). The abundance of oxygen vacancies (OVs) in the photo-anode (i.e., catalyst) has benefitted the e^- trapping of PFOA by the h^+ of the catalyst. This eventually facilitates hole-based PFOA oxidation by charge injection. The introduction of OVs in BiOCl not only offers localized states for trapping photo-generated electrons, but also acts as active sites for adsorbing PFOA, both helped to improve the h^+-oxidation of PFOA (**Figure 5**) [78]. As reported, 2D-rGO is advantageous in charge-carrier separation, whereas the degradation of PFOA decreases from 95.4% to 93.1% increasing rGO content (2 % to 3 %) due to BiOCl shield from absorbing UV light. $BiOX/TiO_2$ photocatalysts (X: Cl, Br, and I) were recently reported with 82 % defluorination efficiency towards PFOA contaminants [79]. Degradation values of PFOA for BiOI, BiOBr, BiOCl were 48 %, 33 %, and 50 % whereas 88 %, 100 % and 96 % for $BiOI/TiO_2$, $BiOBr/TiO_2$ and $BiOCl/TiO_2$ respectively. This signifies the impact of synergism by titanium centres by a two-fold better activity by BiOX systems. The generation of $O_2^{\bullet -}$ due to photo-

induced electrons as well as the photo-induced hole transfer from TiO_2 to BiOX (through the [110] facet) forming a hetero-junction have resulted in better degradation.

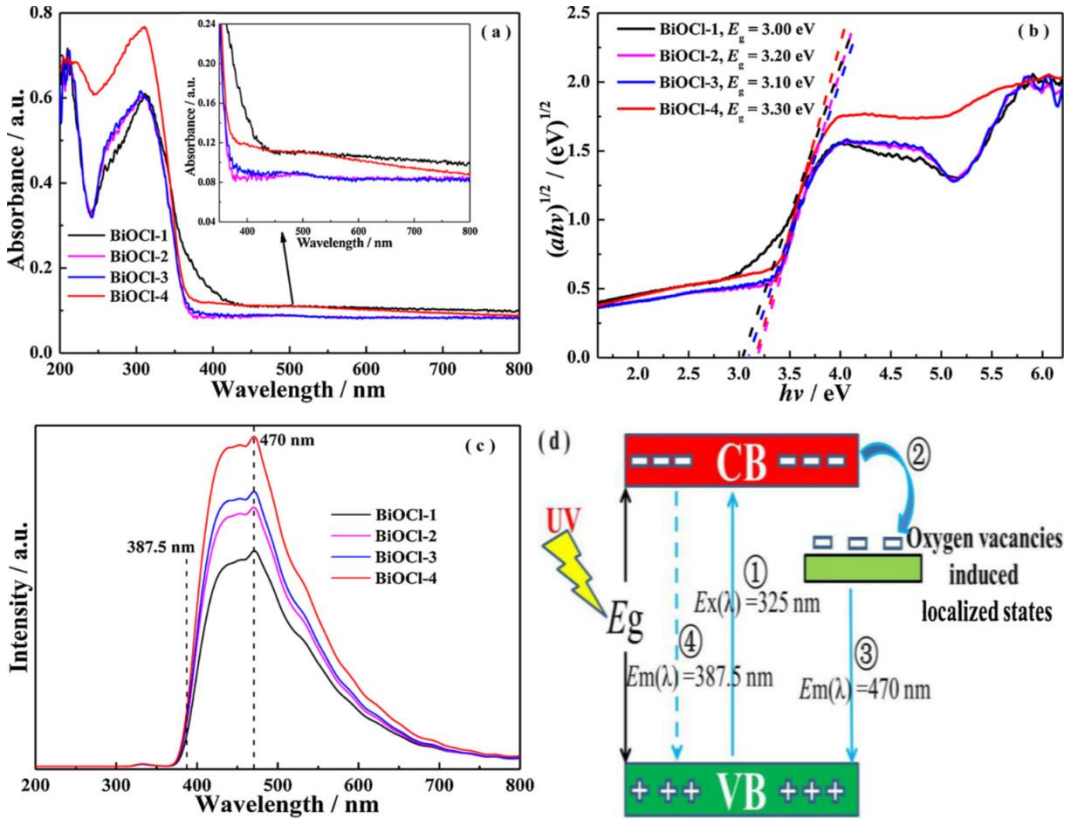

Figure 5. (a) UV–vis DRS spectra, (b) (αhv)1/2 verves hv curves, and (c) PL spectra of BiOCl samples. (d) Photogenerated carriers excitation-recombination process of BiOCl with Oxygen Vacancies (OVs). [78] (Copyright Elsevier).

2.4 Zinc based electrodes

Adding 1 mM zinc chloride ($ZnCl_2$) in the aluminium electrode-based electrocoagulation (EC) process has improved the degradation efficiency from 73.7 % to 99 %. In contrast, zinc oxide (ZnO) does not influence the degradation parameters (reasons are not clear). A clinical synergism in controlling the rise in the pH value (i.e., $Zn(OH)^+$ formation) and improvising the floatation abilities enhanced the PFOA complexation ability through 'Al-F' bonding occurrence in the presence of $ZnCl_2$ [80]. Both flotation-based (i.e., upper floc) and coagulation-based (i.e., lower floc) have shown a two-way methodology in emphasizing the

remediation process. The adsorption of PFOA by the floated flocs seems to exist due to the hydrophobic carbon chain of PFAs. The presence of NaOH (~ 4 mM) and the $ZnCl_2$ (~ 3 mM) has resulted in better treatment of PFOA in treating actual wastewater matrices in the EC process. bA novel treatment train combining electrocoagulation (EC) and electro-oxidation (EO) was verified for long-chain PFASs using zinc (EC) and titanium oxide anodes (EO), respectively [81]. In electrocoagulation, the dissolution of sacrificial anode resulting the formation of cation constituents (e.g., Zn^{2+}) to form hydroxyl complex species (both polymeric and monomeric) towards the sorption of the contaminants. Zinc anodes have provided an appealing performance compared to the other anode materials over the separation of PFASs (e.g., aluminium, iron, magnesium) in aqueous systems. The occurrence of foam was not reported in low current densities and low concentrations of PFAS. At greater than 1 mA cm^{-2}, the optimal values were observed and 0.1 μM. This hybrid process has shown better parameters for PFASs degradation (mainly long-chain) at concentrations ranging from ppt (i.e., ng/l) to ppm (i.e., mg/l) order, with no additional aspects like anode regeneration and contaminants waste. An air cathode-based electrocoagulation (AC-EC) process (Zn anode) has been observed with better removal of PFOA (0.25 mM) and PFOS systems at 69 – 81% lower energy consumptions than conventional EC (EC-aeration) [82]. PFOA was observed with better degradation (71.3 ± 11.3 %) at higher initial concentrations due to the better mass transfer effect relative to low concentration systems (22.6 ± 7.8 %). The various aspects of electrochemical advanced oxidation processes (i.e., Fenton/Coagulation/Oxidation) can be observed in the **Figure 6**.

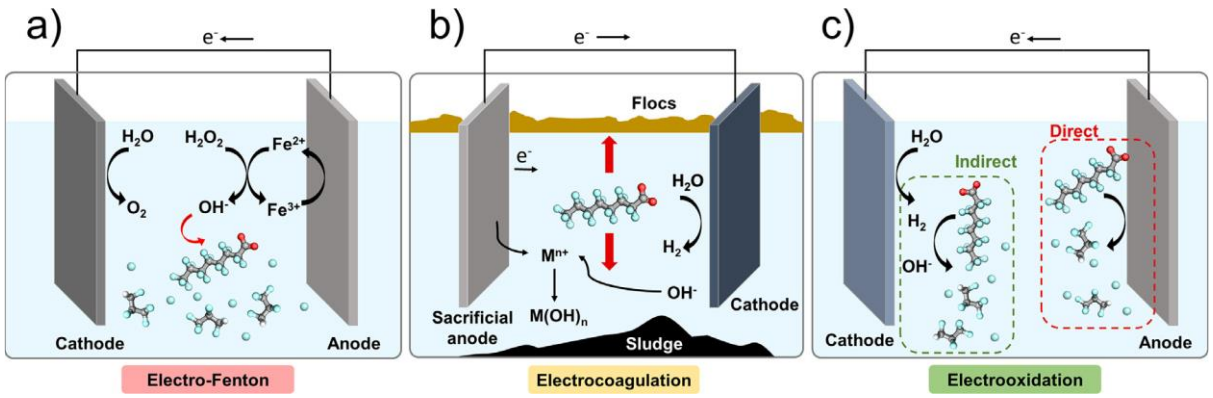

Figure. 6. Electrochemical advanced oxidation processes used for PFAS degradation (a) Electro-Fenton mechanism, (b) electrocoagulation methods and (c) indirect and direct electro-oxidation [37]. (Copyright Elsevier).

2.5 Other metal/metalloid based electrodes

In a recent study, the combined influence of In_2O_3 and persulfate ions ($S_2O_8^{2-}$) under solar light irradiation has been observed with 98.6 % degradation of PFOA after 10 h. The synergistic effect of photons in producing holes and $SO_4^{\bullet-}$/•OH radicals towards hole oxidation as well as surface adsorption have shown an impact on the destructive removal of PFOA (**Figure 7**) [60]. Whereas, In_2O_3 nanoparticles were reported for degrading PFOA in an aqueous solution discussing the impact of various parameters like pH, inorganic anions, catalyst dose, natural organic matter (NOM), and dissolved oxygen (DO) [83]. DO in aliquot systems generally inhibits the recombination of excited electron and hole pairs by accepting electrons in the photocatalytic reactions. The inhibition of PFOA degradation could be attributed to the competitive adsorption of PFOA on the catalyst surface and radical consumption. The interactions between H_2O_2 and chloride ions in the NOM-loaded system positively affected PFOA decomposition, whereas the degradation efficiencies decreased during NOM absence. Co-based oligolayered MXene (Co@o-MXene) achieved complete oxidation of Sodium p-perfluorous nonenoxybenzene sulfonate (OBS) [novel alternative to perfluorooctane sulfonate (PFOS)] with 78.5% oxidation in 2 min reaction time during catalytic ozonation with PMS [84].

A novel gallium oxide (i.e., Ga_2O_3) photocatalyst has been reported for complete degradation of PFOA in UV and Visible spectra assisted by peroxymonosulfate (PMS) [85]. As in previous studies, the efficacy of hydroxyl radicals in the degradation PFASs was observed with a few limitations. PMS would assist in providing better radicals like $SO_4^{\bullet -}$. Two-fold better rate constants were observed for the catalyst (i.e., PMS/ Ga_2O_3) with 185 nm UV-source (60 min) compared to 254 nm UV-irradiation (120 min). In contrast, visible irradiation has little impact on degradation. EPR study findings confirm that • OH radicals are of secondary importance compared with $SO_4^{\bullet -}$and $O_2^{\bullet -}$ radicals in degradation, whereas photogenerated electrons dominated photogenerated holes in promoting the photocatalytic effect.

$$SO_4^{\bullet -} + SO_4^{\bullet -} \rightarrow S_2O_8^{2-} \qquad \text{(Eqn 1)}$$

$$S_2O_8^{2-} + e^- \rightarrow SO_4^{\bullet -} + SO_4^{2-} \qquad \text{(Eqn 2)}$$

Electrochemical-reductive (ER) and Electro-Fenton (EF) treatments are another kind of remediation technique considering the ease of operation and mild reaction kinetics [86] [87]. PFOA degradation efficiencies onto an Rh/Ni electrode (i.e., Rh^{3+} - Ni foil) were observed as 50.4 %, 44.8 %, and 18.0 % in dimethylformamide (DMF), acetonitrile (ACN), and tetrahydrofuran (THF) solvents in ER, respectively. The difference in the ionic conductivity parameters of the individual systems DMF is 4.0 $S \cdot cm^{-1}$, ACN (3.7 $S \cdot cm^{-1}$), and THF (2.4 $S \cdot cm^{-1}$) [25 ℃] has resulted in different degradation efficiencies. The same impact was observed with variation in the supporting electrolytes, where $FeCp_2^*$ [i.e., Bis-Pentamethylcyclopentadienyl-iron(II)] was observed with better degradation parameters concerning other commonly utilized electrolytes like Ammonium fluoroborate (AF), Tetrabutylammonium Perchlorate (TBAP).

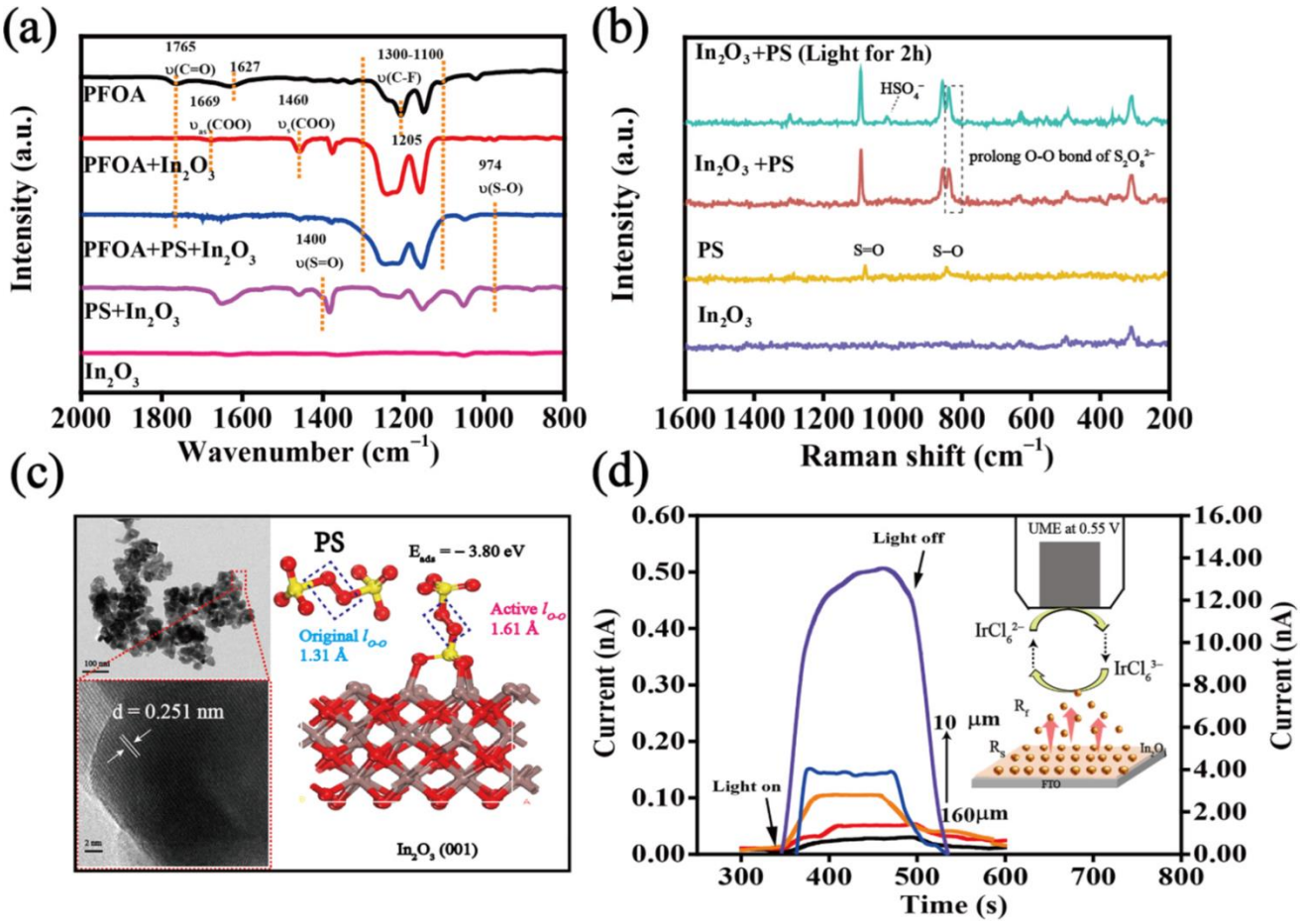

Figure 7. a) The infrared spectrum of In_2O_3, PFOA, In_2O_3/PS, In_2O_3/PFOA and In_2O_3/ PFOA/PS, (b) Raman spectroscopy of In_2O_3, PS, In_2O_3/PS before and after lighting for 2 h, (c) TEM image of the as-prepared In_2O_3 (left) and PS adsorption free energy on the In_2O_3surface (right), (d) Feedback current transients under intermittent illumination of Pt UME of SECM for In_2O_3/PS system. The solution contained 1 mM K_2IrCl_6, 10 mM PS and 0.1 M Na_2SO_4. The potential of Pt UME was 0.55 V vs. Ag/AgCl, and the irradiation time was 200 s. The tip was positioned from bottom to top, 10 (R- Axis), 20 (R- Axis), 40 (R- Axis), 80 (L- Axis) or 160 μm (L- Axis) above the substrate (In_2O_3/FTO). [60] (Copyright Elsevier).

Electro-Fenton (EF) degradation/mineralization was recently reported towards GenX (i.e., Hexafluoropropylene oxide dimer acid) using a graphene-Ni foam (cathode) paired with boron-doped diamond (BDD) electrodes (anode) [87]. EF mechanism is a popular electrochemical advanced oxidation process based on the production of •OH radicals and H_2O_2, whereas it

received limited reactivity while dealing with PFASs ($K_{abs} \leq 10^5$ mol L^{-1} S^{-1}). A direct electron transfer mechanism majorly influences the GenX decomposition behavior compared to the formed •OH radicals in the EF process. An impressive mineralization parameter of around 92.2 % was observed in 6 h of treatment (16 mA cm^{-2}) due to the synergistic effect of EF and BDD oxidation.

Boron nitride (BN) was observed with efficient photocatalytic degradation of PFOA under 254 nm irradiation despite the wide energy band gap of BN electrodes (~ 6 eV) of UVC. The respective half-life and photocatalytic rate of the PFOA species over the BN system is about 1.2 h, and 0.24 mg of PFOA L^{-1} min^{-1}, which are better than TiO_2 parameters (2.4 h, 0.11 mg L^{-1} min^{-1}) [88]. The corresponding de-fluorination values are observed at about ~52% and ~40% for BN and TiO_2 systems (t ~ 4h). Both holes and radical species are involved in the degradation of PFOA and related by-products. The intrinsic and externally introduced (i.e., ball-milling) edge defects or B or N vacancies have improved photocatalytic performance (0.24 to 0.44 mg of PFOA L^{-1} min^{-1} after ball-milling). Flow anodic systems with boron doped diamond (BDD) plate (anode current collector) and Ti-mesh (cathode) electrodes were observed with continuous defluorination of perfluorooctanoic acid (PFOA) with better efficiency (94 %) for 12 days [89]. The combined direct electron transfer (DET), hydroxyl radicals (·OH) mediated oxidation has resulted in better defluorination parameters with a comparable energy consumption of 38.1 Wh mg^{-1}.

The possible application of fluorocarbon constituents in degrading PFASs was also observed recently. A tubular polytetrafluoroethylene (PTFE) doped PbO_2 film anode onto ceramic support has been observed with energy-efficient destruction of PFOA contaminants at ppm-level [90]. The corresponding DFT calculation evidenced the direct electron transfer has initiated the degradation, and further degradation was enabled by hydroxyl radical attack (i.e., •OH). Ceramic/PbO_2-PTFE anode was observed with a 15-fold better reaction rate parameter

(K_{obs}) and around 3-fold in service life compared to a conventional Ti/SnO_2-Sb/PbO_2 anode material. A novel duo-functional tri-metallic-oxide (f-TMO) hybrid photocatalyst (Ti-Ce-Co) was reported with degradation values of > 98.9 % for PFOAs (60 min) and 95.5 % for PFOSs (300 min) and highly regeneration ability up to eight cycles [91].

2.6 Carbon based electrodes

Carbon-based electrode materials have been in good agreement in handling these forever materials. A recent study on the close observation of the influence of activated carbon (AC) and carbon aerogel (CA) in the presence of persulfate (PS) has provided exciting insights [92]. The AC structures with a highly porous behavior have shown adsorption-dominated remediation towards PFOA in the presence and the nascence of the radical source [i.e., PS]. However, the effect of PS on AC structures in the degradation efficiency is negligible most appropriately retrograding (AC ~ 81 %, AC+PS ~ 61 %). But, the aerogel (CA) structures have shown better degradation efficiency with the synergism of PS towards a catalytic activated remediation mechanism due to the combination of surface defects, oxygen-containing functional groups, and sp^2 hybridization assisted in impressive catalytic and charge transfer aspects. The degradation of PFOAs has followed an indirect path in forming intermediates, i.e., shorter-chain PFCAs (PFHpA → PFHeA → PFPeA → PFBA → PFPrA → TFA) while releasing fluorine ions. Metal centres [e.g., Fe(III)O] in carbon spheres (CS) were observed to improvise the photon utilization in the UV band (~ 254 nm) during PFAS degradation against the direct photolysis of PFOA, which requires deep UVC light [73]. The interaction of PFOA onto FeO-CS systems was observed with various mechanisms like electrostatic, hydrophobic, *Π*-electron, ligand exchange, and hydrogen bonding (i.e., hydrophilic). The composite synergistically supported degradation where CS provided the ability to react with hydrophobic tail, and iron centres acted onto hydrophilic head-centres. Carbon sphere (CS) modified bismuth phosphate (BiOHP) has been observed with material synergism towards the complete

degradation of adsorbed PFOA after 4 h under UV irradiation (**Figure 8**) [93]. Without the carbon modification, pristine BiOHP was observed with limited ability towards PFOA defluorination, which may be due to fast recombination of charge carriers (e^-, h^+), and the competition of water molecules for the photogenerated h^+.

The stability of hydrated electrons generated during the experiments plays a crucial role in the degradation, but the dissolved oxygen and other co-contaminants tend to consume these radicals. To overcome this, a cationic surfactant (CTAB) for stable and self-assembled micelles has been reported to prevent the quench impact on Hydroxyphenylacetic acids (HPAs) generated by hydrated electrons by oxygen/proton species during degradation [94]. Three HPA isomers (2-HPA, 3-HPA, and 4-HPA) were verified for HFPO-TA degradation with CTAB, where the surfactant reduced the intramolecular electrostatic repulsion. A tiny micelle generally indicates a tighter structure protecting the generated hydrated electrons (2-HPA: 9 nm, 3-HPA, and 4-HPA: 20 nm). But, passive hydrated electrons decay parameters of 4-HPA ($t \sim 2124$ ns) to other isomers (1527 - 2037 ns) resulted in better defluorination despite the larger micelle size to 2-HPA. A clear impact of pH was observed in the degradation in the range of 4 - 10. An impressive defluorination was observed at pH 6 for all the isomers (26 - 28 %), whereas the decomposition was reduced in larger pH systems (pH 10), especially for 3-HPA and 4-HPA.

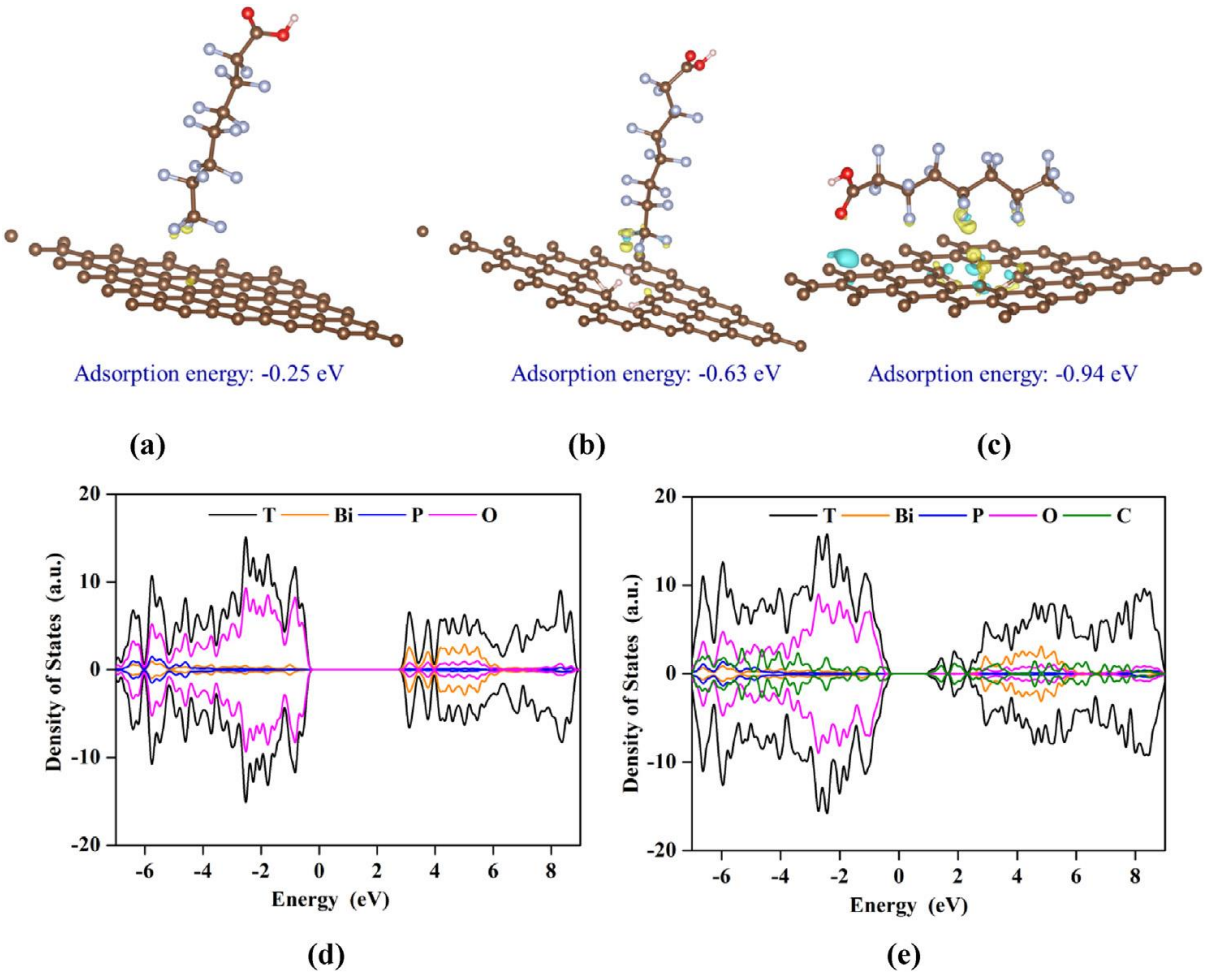

Figure 8. Optimized adsorption modes and charge density distributions of PFOA on CS (a), defective CS with end-on configuration (b) and sideon configuration (c); Density of states of neat BiOHP (d) and BiOHP/CS (e). Yellow: charge accumulation, blue: charge depletion, T: Total; Iso-surface = 0.0005. (For interpretation of the references to color in this figure legend, the reader is referred to the web version of this article.) [93] (Copyright Elsevier).

Kugler et al. developed an effective method of degrading PFOS by hydrated electrons (e_{aq}^-) that are generated from 3-indole-acetic-acid (IAA) upon UV irradiation onto 12-amino lauric acid (ALA) intercalated montmorillonite [95]. ALA entering the interlayer region of montmorillonite increases interlayer spacing and surface sites where the IAA and PFOS are co-adsorbed. During UV irradiation, the hydrated electrons and indole radical cations are

emitted at IAA, resulting in PFOS degradation. During the degradation, the H/F exchange pathway has dominated the C-C cleavage and desulfonation processes for the PFOS system.

3. Degradation Mechanism and Pathways

The PFOA degradation in the electro-oxidation mechanism for titanium suboxide (TSO) was observed with the electron loss from a carboxyl group and the formation of the perfluoroalkyl radical through radical hydroxyl oxidation and subsequent decarboxylation. The mineralization of PFOA to CO_2 and HF was observed through hydroxide radicals and direct electron transfer, where the •OH species was observed with a major role [61]. Decarboxylation followed by the oxidation pathway is the major degradation pathway in photoelectrochemical (PEC) systems over electrochemical (EC) studies. The direct electron transfer (DET), •OH oxidation, and radical chlorine species (RCS) took a significant role in degradation in PEC. DET, •OH, and RCS contributions with a graphene oxide – TiO_2 anode were observed as 55.4, 15.1, and 29.5 %, and 29.9, 53, and 17.1 % in PEC, EC systems, respectively [65]. In corresponding to the iron electrode materials, mixed oxidation of the iron centres plays a significant role in the generation of the radical species (oxygen, e^-, and h^+). In Fe-doped zeolites, the impact of molecular oxygen is understood with three reactions influencing the degradation pathways, like (i) As a source for reactive species (•OH and HO_2•), (ii) Facilitates the re-oxidation of Fe(II) to Fe(III), and (iii) molecules oxygen are directly involved in the complex radical chemistry of PFCA degradation (Eqn 3-4) [69]. Fe(III) centres in iron oxide and carbon spheres were found to influence the degradation process with better complexation with PFOA species in enhancing the light absorption and facilitating electron transfer (i.e., redox process) as observed in **Figure 9** [73]. Fe(III) centres formed by PFOA oxidation activate oxygen towards ROS (i.e., •OH), promoting PFOA photo-degradation in transforming intermediates to perfluorinated alcohol. DFT calculation of PFOA onto Fe/TNTs@AC observed with direct hole oxidation initiated the

degradation in activating the PFAS molecule followed by the series of decarboxylation/defluorination pathways (i.e., C–F bond cleavage) [66].

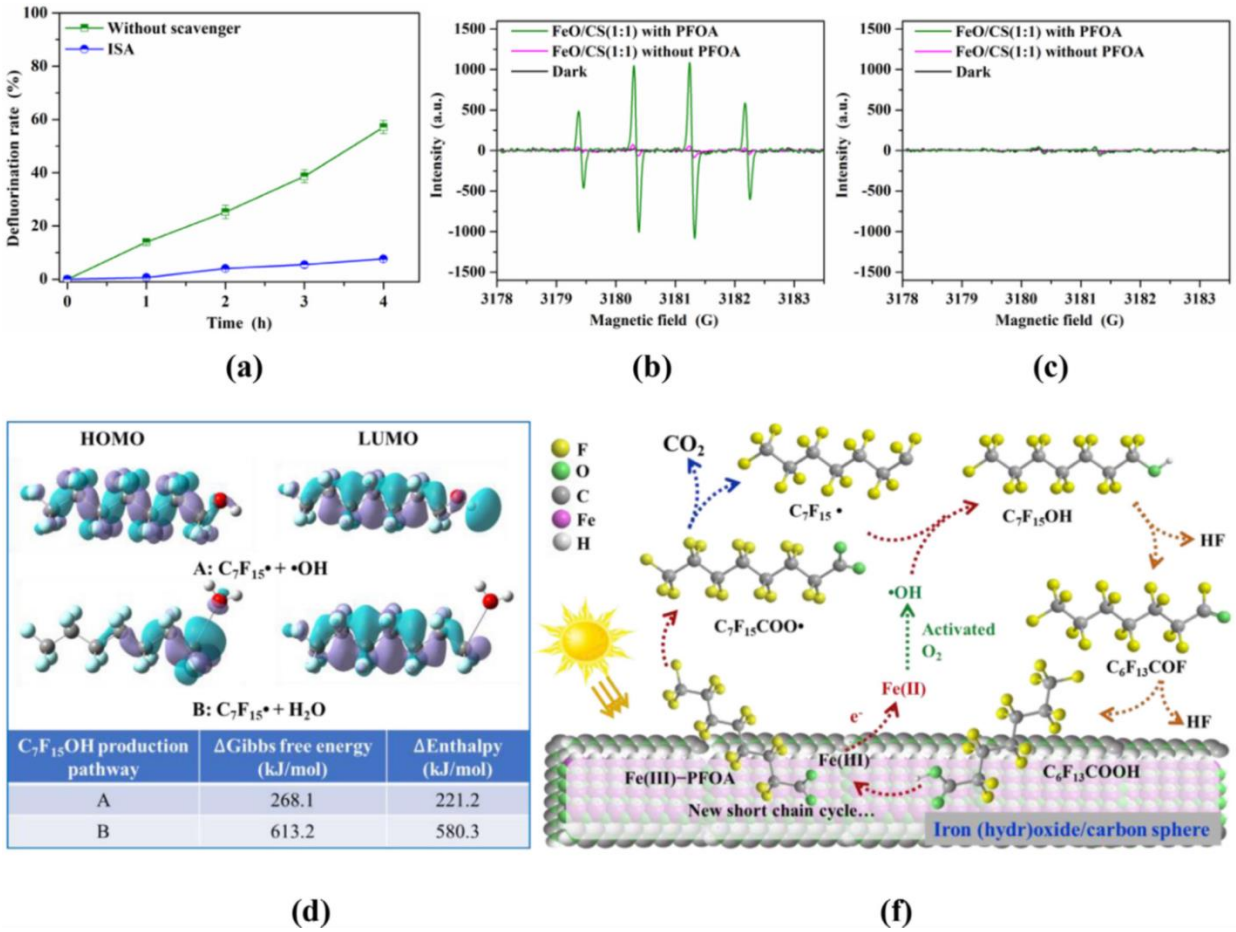

Figure. 9. Defluorination rate of PFOA by FeO/CS(1:1) with or without ISA (a); EPR spectra of DMPO–%OH adducts produced by FeO/CS(1:1) under air (b) or Ar (c) with or without PFOA and upon solar light irradiation for 20 min; The iso-surface plots of frontier orbitals of C_7F_{15}• when combined with •OH or H_2O, and the corresponding Gibbs free energy change at 298.15 K and reaction enthalpy change (d). The purple and blue iso-surfaces represent charge accumulation and depletion in the space, respectively; Proposed pathway of PFOA degradation by FeO/CS under solar light (e). [73]. (Copyright Elsevier).

In a recent study, indium doped activated carbon-supported titanate nanotubes (TNTs@AC) were observed with > 99 % of PFOA degradation in 4 h under optimal conditions (25 ◦C, pH

7, 1 atm, 1 g/L catalyst, 0.1 mg/L PFOA, 254 nm) [96]. The doping has resulted in the generation of local positively charged sites for PFOA adsorption followed by photo-degradation. The substitution of In^{3+} for Ti^{4+} in titanate formed oxygen vacancies that effectively separated e^- and h^+.

$$C_nF_{2n+1}COO^- + Fe^{3+}\text{-zeolite} \leftrightarrow [C_nF_{2n+1}COO\text{-}Fe]^{2+}\text{- zeolite} \quad \text{(Eqn 3)}$$

$$[C_nF_{2n+1}COO\text{-}Fe]^{2+}\text{-zeolite} \xrightarrow{UVA} C_nF_{2n+1}COO\bullet + Fe^{2+}\text{- zeolite} \quad \text{(Eqn 4)}$$

Enlarged surface area parameters, better UV-light absorption, and efficient separation of electron-hole pairs due to the high-exposure (001) facet in $BiOI_{0.95}Br_{0.05}$ promoted the photocatalytic activity towards PFOA degradation [75]. The better photo-current density of 0.11 - 0.15 μA cm^{-2} and radical species (•OH, $\bullet O_2^-$, and h^+) have synergistically influenced the PFOA degradation [76]. The decarboxylation process is initiated by h^+ in BiOCl/rGO nano-composites to yield unstable perfluoroheptyl radicals ($\bullet C_7F_{15}$) that react with •OH to form $C_7F_{15}OH$, which transforms into shorter-chain intermediates (i.e., perfluorocarboxylic acids), in facilitating the PFOA degradation [77]. The detailed EPR analysis of CS modified bismuth phosphate confirms the better intensity of $O_2\bullet^-$ in the composite has synergized the adsorption and corresponding photo-degradation. A two route mechanism was observed for graphene-Ni foam paired with boron-doped diamond electrodes in Electro-Fenton (EF) treatment [87]. Where the dissociation through electron transfer was initiated either in the carboxylic group or in the ether group, where the ether group was observed with the lowest dissociation energy in GenX (~ 212.8 kJ mol^{-1}).

Sulfate-free radicals attacked PFOA to initiate a decarboxylation reaction for the carbon aerogel and persulfate (PS) system in forming perfluoroalkyl radicals (i.e., $C_nF_{2n+1}\bullet$) [92]. The perfluorinated radical in a continuous reaction with $SO_4^{\bullet-}$ to form the unstable $C_nF_{2n+1}OSO_3-$. which hydrolyses to perfluorinated alcohols ($C_nF_{2n+1}OH$) followed by HF elimination in developing $C_{n-1}F_{2n-1}COF$. $C_{n-1}F_{2n-1}COF\bullet$ transforms to $C_{n-1}F_{2n-1}COOH$ through further

hydroxylation, and the cycle continues until the elimination of the fluorine molecule in providing short-chain PFASs and fluoride mineralization (i.e., F^-). Decomposition of PFOA to fluoride ions (i.e., $C_6F_{13}COOH \rightarrow C_5F_{11}COOH \rightarrow C_4F_9COOH \rightarrow C_3F_7COOH \rightarrow C_2F_5COOH \rightarrow CF_3COOH$) with 85.7 % efficiency at a pH of 3.8 (60 ^{O}C). The addition of PS has decreased the corresponding activation energies of PFOA (66.8 to 37.2 kJ/mol) removal and defluorination (97.3 to 49.2 kJ/mol). The activation of PS (light/heat/activators, e.g., metal-centers) has resulted in providing free radicals ($SO_4^{\bullet-}$) in the degradation of PFOA through a better hole-electron separation by accepting electrons in the CB of BiOHP (Eqn 5-6) [93]. This phenomenon provides the availability of holes in assisting the direct hole-oxidation of PFOA. The density of states (DOS) study observes that CS lowers the energy required for electron transition in the photocatalytic/degradation process.

$$S_2O_8^{2-} + \text{heat (or) light} \rightarrow 2SO_4^{\bullet-} \quad \text{(Eqn 5)}$$

$$S_2O_8^{2-} + \text{activator} \rightarrow SO_4^{\bullet-} + SO_4^{2-} \quad \text{(Eqn 6)}$$

Short-chain perfluorinated carboxylates (i.e., PFHpA: $C_6F_{13}COO^-$, PFHxA: $C_5F_{11}COO^-$; and PFPeA: $C_4F_9COO^-$) were detected using Rh/Ni cathode in electrochemical reductive decomposition (ERD) experiment. The ERD process towards PFOA involves mechanisms like 'Approach/adsorption at the cathode', 'Generation and transfer of highly reductive species (e.g., Rh chemisorbed H*), and 'Occurrence of the hydrodefluorination (HDF) reaction (**Figure 10**) [86]. The decomposition has been initiated at the α-position of the C-F bond in the PFOA molecule. The unstable α-position carbon atom gets reacted with the continuous supply of the electrons. This process resulted in a decarboxylation reaction by forming COO^- and $C_6F_{13}^-$ radicals and losing a carbene function. The individual concentrations of the short-chain compounds and the NMR spectroscopy analysis implicate a step-wise decomposition of the

PFOA through the transformation of [–CF_2–CF_2–] bonds to [CF_2–CHF–] or [–CF_2–CH_2–] bonds.

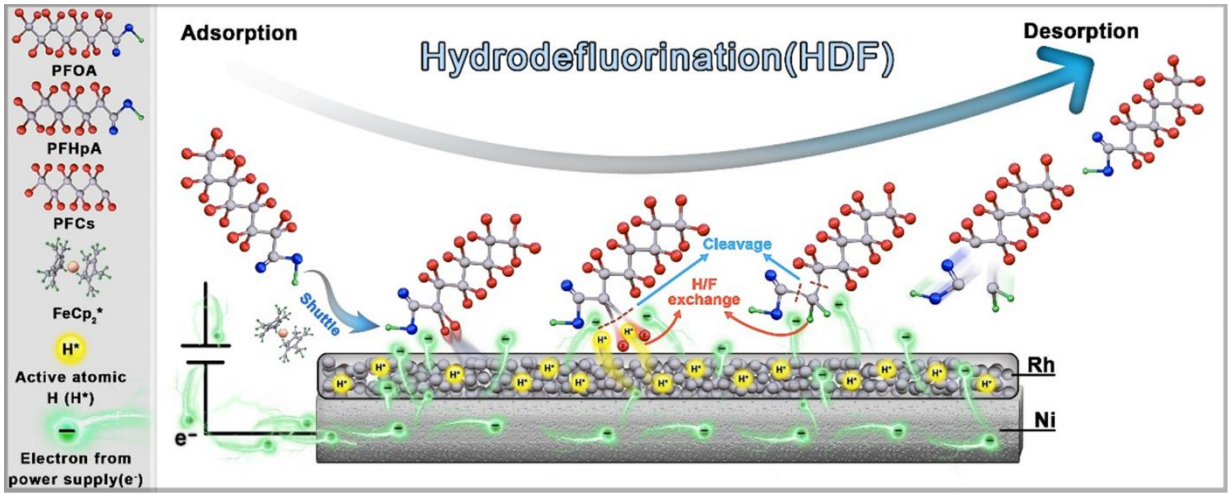

Figure 10. Proposed mechanisms for the hydrodefluorination of PFOA on Rh/Ni cathode [86]. (Copyright Elsevier).

A synergistic module of heterogeneous and homogenous catalytic reactions onto PFOA with In_2O_3/PS systems has been observed with activation of PFOA via direct hole oxidation [60]. The activation of PS adsorbed onto In_2O_3 by capturing the photogenerated electrons resulted in the separation of electrons and holes in the photocatalyst (In_2O_3), facile mass transportation between PS and the activators, and also producing high radical yields ($SO_4^{\bullet-}$ and ·OH). SO4• easily attacks the perfluoroalkyl radicals $(C_7F_{15}\bullet)^-$, resulting in conversion to $C_7F_{15}OSO_3^-$, which is readily hydrolyzed to perfluorinated alcohols (i.e., $C_7F_{15}OH$) followed by a series of intramolecular rearrangements including a hydrolysis reaction and HF elimination, resulting in the formation $C_{n-1}F_{2n-1}COOH$. The presence of NO_3^- and humic acid have shown mixed behavior towards defluorination, where the former improved the efficiency due to the reactive nitrogen species (RNS) and the latter diminished the effect (reaction with radicals). A strong affinity of the surface of ceramic/PbO_2-PTFE towards PFOA assisted the easy transfer of PFOA from bulk to the electrode, resulting in a better performance than Ti/SnO_2-Sb/PbO_2 [90].

The degradation pathway was initiated by the direct electron transfer (DET) in cleaving the –COO- followed by the reaction between perfluoroalkyl and oxygen radicals (C_nF_{2n+1}• and •OH/O_2/H_2O).

Iridium pentoxide (Ir_2O_5) plating titanium electrode was observed with no short-chain PFSAs (PFCA/PFSA) during electrochemical treatment of the saturated soil contaminated with PFOA [97]. The total degradation ratio and defluorination values after a 10-day treatment are observed to be around 51.7 %, 44.7 % for PFOA, and 33 %, 23 % for PFOS. The degradation of the PFOA is explained in two different pathways over the formation of the perfluoroheptyl radical by the influence of the hydroxyl radical (path A: Eqn 7-10) and the dissolved oxygen near the electrode (path B: Eqn 11-12). The degradation of the PFOS species was due to the e- loss to the anode by direct oxidation and the formation of a PFOS radical (Eqn 13-14). This PFOS radical proceeds to desulfation in the formation of C_8F_{17}•, and the cycle repeats towards the mineralization. PFAS degradation mechanism occurs mainly at the anode for oxidation, while desorption and mobilization occur throughout the reactor. The cumulative action of destruction, desorption, and mobilization mechanisms in soil has resulted in the better removal of PFASs.

$$C_7F_{15}\bullet + \bullet OH \rightarrow C_7F_{15}OH \quad \text{(Eqn 7)}$$

$$C_7F_{15}OH + \bullet OH \rightarrow C_7F_{15}O\bullet + H_2O \quad \text{(Eqn 8)}$$

$$C_7F_{15}O\bullet \rightarrow C_6F_{13}\bullet + CF_2O \quad \text{(Eqn 9)}$$

$$CF_2O + H_2O \rightarrow CO_2 + 2HF \quad \text{(Eqn 10)}$$

$$C_7F_{15}\bullet + O_2 \rightarrow C_7F_{15}OO\bullet \quad \text{(Eqn 11)}$$

$$C_7F_{15}OO\bullet + RCOO\bullet \rightarrow C_7F_{15}O\bullet + RCO\bullet + O_2 \quad \text{(Eqn 12)}$$

$$C_8F_{17}SO_3^- \xrightarrow{e-} C_8F_{17}SO_3\bullet \quad \text{(Eqn 13)}$$

$$C_8F_{17}SO_3\bullet + H_2O \rightarrow C_8F_{17}\bullet + SO_4^{2-} + 2H^+ \quad \text{(Eqn 14)}$$

Fe-Zeolites for PFOS degradation are observed with a combined influence of adsorption and photocatalytic effect through a sulfonate-to-metal electron transfer process generating $C_8F_{17}SO_3^{\bullet}$ [70], a similar process followed with the Ir_2O_5 systems [97]. Whereas terminal oxygen has played a significant role in the formation of the hydroxyl radical species in receiving support from the mixed iron oxide centres (**Figure 11)** [Eqn 15-17].

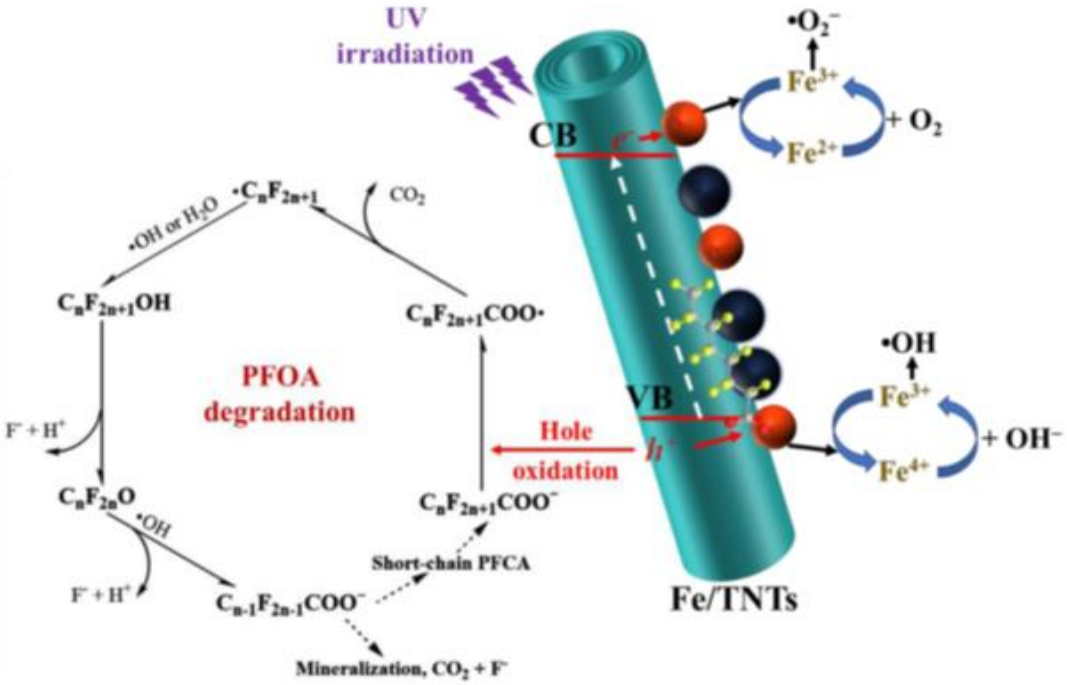

Figure. 11. Conceptualized illustration of photocatalytic reaction mechanisms of Fe/TNTs@AC [66]. (Copyright Elsevier).

$$Fe^{2+}\text{-zeolite} + O_2 \rightarrow Fe^{3+}\text{-zeolite} + \bullet O^{2-} \quad \text{(Eqn 15)}$$

$$Fe^{2+}\text{-zeolite} + \bullet OH \rightarrow Fe^{3+}\text{-zeolite} + OH^- \quad \text{(Eqn 16)}$$

$$Fe^{3+}\text{-zeolite} + H_2O \xrightarrow{UV} Fe^{2+}\text{-zeolite} + \bullet OH + H^+ \quad \text{(Eqn 17)}$$

In $PMS/Ga_2O_3/UV$ system, out of five types of possible active species (i.e., $SO_4\bullet^-$, photo-induced holes and electrons, •OH, and $O_2\bullet^-$), photogenerated electrons, sulfate, and oxygen radicals have shown an impressive performance [85]. Sulfate radical anions and super-oxide

ions can oxidize PFOA into perfluorinated alkyl radicals (•C_7F_{15}), thereby providing $C_6F_{13}COF$ and HF elimination. The further hydrolysis of $C_6F_{13}COF$results in intermediated products $C_6F_{13}COOH$ (PFHpA). The PFOA transformation over TiO_2-rGO photocatalyst is from the individual (or) the combination of direct reaction (photogenerated holes) and indirect reaction (hydroxyl radicals) in producing PFHpA followed by complete mineralization and de-halogenation [64]. A schematic representation of photocatalytic degradation pathway of PFOA onto titanium metal oxide systems ($BiOCl/TiO_2$) is provide in **Figure 12.**

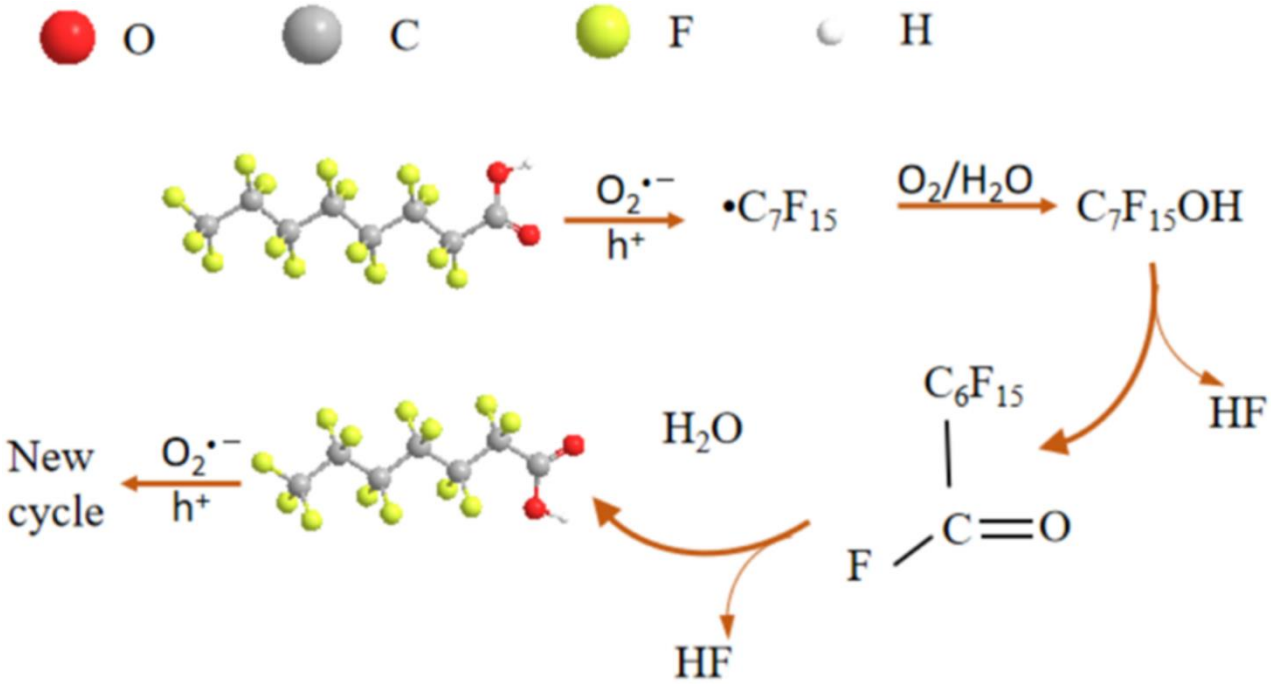

Figure 12. Illustration of the photocatalytic degradation pathway of PFOA over $BiOCl/TiO_2$ [79]**.** (Copyright Elsevier).

4. Pilot Studies and Field Level Applications

A two-step 'Concentrate-&-Destroy' technology using an adsorptive photo-catalyst (Fe/TNTs@AC) was reported for treating over 18 PFAS with 92 % removal efficiency from a model municipal landfill leachate through various bench- and pilot-scale studies **(Figure 13**) [98]. Electrokinetic remediation (EKR) can be a viable field-level treatment for PFAS-contaminated soils, either as an individual processor in treatment-train. In a recent study,

Niarchos et al. observed better electrokinetic in-situ soil remediation treatment [99]. Electro-migration is observed to vary with the individual chain length and functional group-specific, where up 89 % removal efficiencies (99 % for $C \leq 6$) are noted with a two-compartment process (Soil chamber, IX resin, and Electrolyte filled chamber) where 75 % was observed with single compartment. About 70 % of the total PFASs were concentrated in the close region of the anode (within 5 cm) in the two-compartment system, and the influence of current density was not observed in the electro-migration.

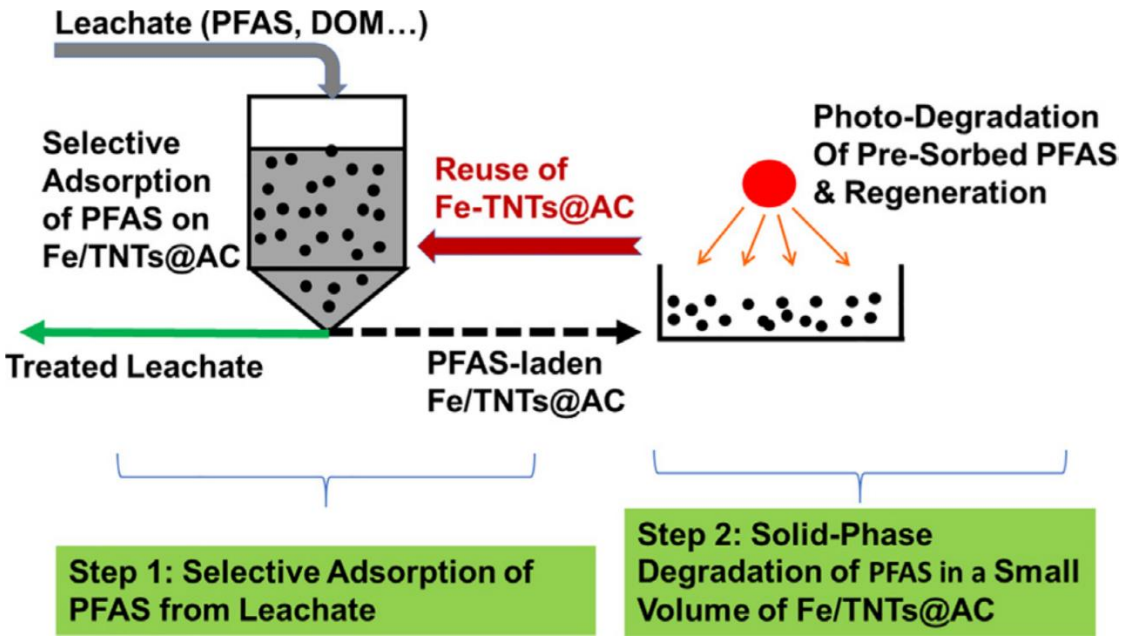

Figure 13. A scheme of 'Concentrate-&-Destroy' technology for enhanced removal and destruction of per- and polyfluoroalkyl substances in municipal landfill leachate. [98] (Copyright Elsevier).

Apart from the metal-based systems, silica-based systems are also reported for the PFASs remediation studies. A coupled photocatalytic alkaline media as a remediation technology was utilized for PFASs in aqueous film-forming foam impacted storm water containing 17 untargeted PFASs [100]. A combination of silica-based granular media (SGM) containing

titanium dioxide under a UV light source and in the presence of sodium hydroxide/thiosulfate has provided better remediation efficiency. The synergism of photocatalytic and nucleophilic attack enhances the remediation abilities, allowing the sulfonate functional head to get cleaved and replaced with an alcohol group, resulting in a carboxylic acid upon stabilization. In the absence of the nucleophilic additives ($Na_2S_2O_3$/NaOH), the degradation efficiencies of the SGM were degraded to about 40 % from 60 - 80 %. The tortuous internal porosity of the SGM has prevented the fouling, which has provided a better performance over other photocatalytic treatment systems.

UV-sulfite treatment of Nano Filtration (NF) treated water samples has been observed with promising behavior for a pilot-scale study in a 30-day period [101]. Where 90 % recovery with the permeate in NF resulted in 75 and 90 % degradation with 4 and 8 h durations respectively, at 10 mM sulfite (pH ~ 11.2). The corresponding PFCA compounds have shown no significant influence of chain length over degradation, whereas PFSA was better degraded with increased chain length. The corresponding energy per order magnitudes (EE/O) of short-chain compounds were observed to be 7 folds higher (> 100 kWh/m^3) than long-chain compounds (13 - 14 kWh/m^3). The corresponding EE/O values of various remediation techniques and electrode materials are provided in the Table 1. Wastewater samples from a municipal sewage treatment plant in Sydney, Australia, were analyzed for PFOA degradation using a novel PMS/ Ga_2O_3 photocatalyst system under UV irradiation (185 nm and 254 nm) [85]. Samples collected from the influent and effluent and photo-degradation of PFOA under the optimum conditions (1.23 g L^{-1} PMS, 0.25 g L^{-1} Ga_2O_3, pH 3) were conducted. Under 254 nm UV irradiation, 100 % PFOA in wastewater was degraded within 120 min with the rate constant of 0.012 min^{-1}, whereas 185 nm UV irradiation was observed with 60.75 % removal at 30 min and 100 % degradation within 60 min. In addition, for effluent, 75 % of total organic carbon (TOC) was removed with 254 UV light, whereas 32 % of TOC was removed with 185 nm UV light. For

the influent sample, 85 % TOC removal was observed with 254 nm UV and 54 % TOC removal with 185 nm UV. Better propagating parameters of 254 nm supported over efficient TOC treatment, the corresponding absorption numbers for wastewater samples are observed around 99 % (185 nm) and 48 % (254 nm).

Table 1. Energy per order magnitude (EE/O) parameters of degradation processes towards various PFASs

Method/electrode	Experimental conditions	Energy consumption	Ref
Ceramic/PbO_2-PTFE	800 mL of 20 mg L^{-1} PFOA, 2.1 g L^{-1} Na_2SO_4, current density (J): 15 mA cm^{-2}	58.54 Wh L^{-1}	[90]
Ti/SnO_2-Sb/PbO_2	800 mL of 20 mg L^{-1} PFOA, 2.1 g L^{-1} Na_2SO_4, J: 15 mA cm^{-2}	160.81 Wh L^{-1}	[90]
EF-BDD	GenX (0.25 mM = 86.8 mg L^{-1}); Batch electrolytic cell, V = 0.08 L, Gr-Ni-foam cathode, BDD anode, j = 16 mA cm^{-2}, pH = 3, Fe^{2+} = 0.2 mmol L^{-1}, K_2SO_4 = 0.05 mol L^{-1}	37.5 kWh m^{-3}	[87]
Si/BDD	PFAS ~ 1,652 μgL^{-1}	101 kWh m^{-3}	[102]
Nano/micro Ti_4O_7 anodes	PFOS = 2 μM, supporting electrolyte 100-mM Na_2SO_4	3.67 - 4.67 kWh·m^{-3}	[62]
Magn´eli phase titanium suboxide	2.0 μM PFOA, 20 mM Na_2SO_4 supporting electrolyte, J: 8.0 mA cm^{-2}	15.8 – 45.5 kWh·m^{-3}	[61]
indium oxides (254 nm)	N/A	2106 kWh·m^{-3}	[41]
nanofiltration (NF) and UV-sulfite photochemical treatment	PFCA	13.1 kWh·m^{-3}	[101]

	PFOS	14.1 kWh·m^{-3}	
	Short chain PFSA	> 100 kWh·m^{-3}	
UV/Sulfite Treatment (185 nm)	PFCA (0.025 mM), Na_2SO_3 (10 mM), carbonate (5 mM)	PFNA: 13.7 (pH 12) – 77 (pH 9.5) kWh·m^{-3} PFOA: 15 .8 (pH 12) – 122 (pH 9.5) kWh·m^{-3}	[103]
Low-cost graphene sponge electrodes	PFOA/PFOS: 0.2 µM, J: 230 A m−2; 10 mM phosphate buffer (Na_2HPO_4/NaH_2PO_4, pH 7.2, 1 mS cm^{-1})	10.1 ± 0.7 kWh m^{-3}	[104]
$BiOCl/TiO_2$	PFOA: 10 mg L^{-1}	640 kWh m^{-3}	[79]
UV/Iodide system	F-53B (alternative to PFOS): 0.5 – 20 µg L^{-1}	365.5 – 102.1 kWh m^{-3}	[105]

Bao et al., reported periodically reverse electrocoagulation (PREC) using the Al-Zn electrodes for remediating PFSA in groundwater samples [both synthetic and natural: fluorochemical industrial park (FIP) in Fuxin of China] [106]. The influencing parameters are observed in the order of 'voltage > pH > stirring speed' through orthogonal experiments. The removal efficiencies in the synthetic aqueous solutions and natural groundwater are of 87.4 %, 95.6 %, 100 % (synthetic) and 59.0 %, 88.2 %, and 100 % (natural) for PFBS, PFHxS, and PFOS respectively. SEM-EDS analysis provides the porous and aggregate floc characteristics with various elemental presences, i.e., O (68.1 %), Al (21.2 %), C (4.16 %), N (4.97 %), Zn (3.43 %), and F (3.29 %) confirming the adsorption of PFSA on the Al-Zn hydroxide floc aggregates. Fe-Zeolite systems were tested for treating both underground and synthetic water samples with a pre-concentration of PFOS around 46 nM and the presence of inorganic co-contaminant

($C_2SO_4^-$ ~ 5.6mM). Surprisingly the influence of sulfate ions was observed with no interference on removal ability in real samples, whereas synthetic water samples were observed with inhibition; this may be due to the complexation issues (i.e., PFOS-Fe^{2+}/Fe^{3+}) [70]. In a recent report, electrochemical oxidation (100 mA/cm^2) of PFASs with boron-doped diamond (BDD) electrode in a real semiconductor Fab industrial wastewater sample showed the degradation of sulfonic functional PFASs was more kinetically favorable compared with carboxylic group PFASs [107]. The short-chain compounds were degraded efficiently in lower pH environments, and the process performance was decreased in the presence of organic surfactants (e.g., SDS and TMAH). A better degradation value was observed for multi-component/contaminant system (i.e., combined C8: PFOA, PFOS; C6: PFHxA and PFHxS; and C4: PFBA and PFBS) compared to single solute systems (i.e., C8/C4). This is due to the increased surface wettability of the electrode surface or lower contact angle.

5. Influencing parameters

5.1 Electrode potential, Current, and Composition

Electrode potential (cathode/anode) observes to be the driving force for the charge transfer process in electrochemical-based contaminant treatment systems. Electrode potential has shown an impact on the degradation with Rh/Ni electrode (i.e., Rh^{3+} - Ni foil), an increase in the degradation was observed for potentials from − 0.20 to − 1.25 V (i.e., − 0.20, − 0.58, − 1.25). In contrast, the diminishing behavior occurred at - 2.2 and - 3.5 V. A high cathode potential resulted in the subsequent accumulation (supporting electrolyte) and precipitation of the decomposition products near the electrode resulting in passive decomposition (**Figure 14**) [86]. The optimal potential bias for BiOCl/rGO nanocomposites towards PFOA degradation was observed around 2 V, implying an optimal bias potential for the generation of •OH (1 V < 2V > 3V) [77]. Higher bias potential promotes the electrochemical production of H_2O_2 from O_2 at the cathode in the EC process, but the excessive H_2O_2 can hinder the process by radical

scavenging. Whereas the influence of the applied voltage (0.5, 0.7, and 1.0 V) has not been observed for both PFOA and PFOS for electrocoagulation (EC) based remediation with an air-cathode [82].

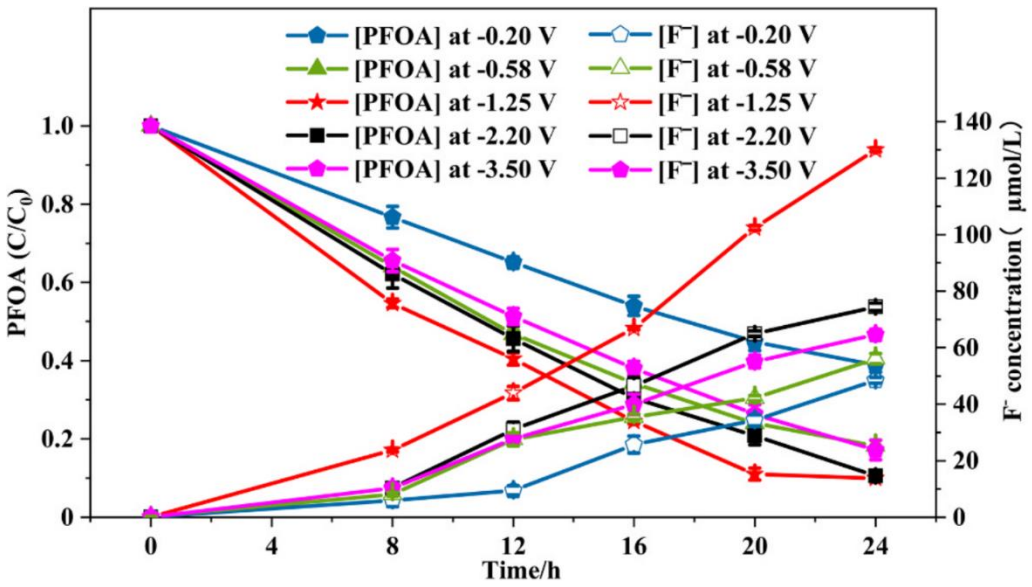

Figure 14. Changes of relative PFOA concentration and F^- concentration in the electrochemical decomposition experiments applied different cathode potential. Experimental conditions: WE, Rh/Ni cathode (2 × 2.5 cm^2); CE, Pt anode; RE, Ag/AgCl; [PFOA]0 = 100 mg/L; [$FeCp_2$]0 = 3 mM; solvent, DMF; agitation force, 400 rpm*. [86] (Copyright Elsevier).

Graphene-coated Ni-foam and BDD Electro-Fenton (EF) reaction experienced better TOC decay when the current density increased from 8 to 16 mA cm^{-2} (49.2 ± 7.1% to 92.2 ± 1.0%). It is reported that the kinetics controlled the process in lower densities, whereas the mass transport influenced the higher densities [87]. The degradation rate of PFOA onto ceramic/PbO_2-PTFE anode was observed about nine times higher at 3.0 V (vs Ag/AgCl) compared to 2.5 V, whereas negligible values were reported at 1.5 and 2.0 V [90]. The GOP25/FTO anodes showed PFOA degradation in the 4 - 6 V potential window where significant PFO rate constants are observed around 0.004 min^{-1} (4 V) and 0.006 V (6 V), whereas it was < 0.001 min^{-1} for 3 V and 4 V [65]. The corresponding current densities are

observed in the range of 1-17 mA cm^{-2} for the voltage window of 3 - 6 V. A better degradation value at higher potentials is due to the increase in the electrode potential, which retards the electron-hole recombination rate in the generation of radical species (e.g., ROS) eventually emphasizing the process parameters. Electro-oxidation with a titanium sub oxide (TSO) membrane anodes reported with degradation efficiencies for PFOA and GenX around 73.9 ± 3.5 % (8.0 mA cm^{-2}), 19.9 ± 5.0 % (1 mA cm^{-2}), and 51.7 ± 8.2 % (8.0 mA cm^{-2}), 12.5 ± 7.1 % (1 mA cm^{-2}) [61].

The composition of the electrode materials also has a substantial impact on PFOS degradation as the redox and charge transfer properties are electrode specific during the electrochemical/ photo-electrochemical process. In observing the PFOS degradation onto titanium sub-oxides (TSO), micro and nano-Ti_4O_7 have exhibited better efficiency to Ebonex anode material (Ti_9O_{17}) [62]. The corresponding lower Mulliken charges (low-electron transfer) and higher adsorption energies (strong sorption) for Ti centres in Ti_4O_7 over Ti_9O_{17} resulted in better degradation. Boron doped diamond (BDD) anode showed better degradation of GenX by pairing graphene-coated Ni-foam cathode with respect to Pt, and fluorine-doped tin oxide (FTO) anodes due to superior charge transfer and electrochemical abilities [87]. The presence of graphene in the TiO_2/FTO anodes was observed with the enhancement in the PFOA degradation efficiency (0.0134 min^{-1}) compared to the pristine anode (0.0109 min^{-1}) [65]. An enhancement in the electrochemical double-layer capacitance and the specific capacitance of the anode in the presence of graphene (5 wt. %) have influenced the degradation rate values.

5.2 Impact of dosage (catalyst)

The appropriate amount of the catalyst influences the respective degradation process due to an increase in the number of reactive sites, whereas an excessive loading might inhibit the final output. In a recent study, the dosage of In_2O_3 in In_2O_3/persulfate system (solar irradiation) has shown better parameters from 0.01 to 0.05 g/L [60]. Under different loading

values of Ga_2O_3 at 2.65, 0.55, 0.25 and 0.10 g L^{-1} with respect to 1:1 molar ratio of per-sulfate (4.35, 0.90, 0.41 and 0.15 g L^{-1}) observed with 100 % PFOA degradation at 0.25 g/L [85]. Fe(TPFPP)/BC catalyst under different loadings (i.e., 0, 0.1, 0.2, 0.5, 1, 2 g/L) where an the degradation efficiencies are observed around 36.96 % to 87.33 % from 0.1 to 1 g/L with no significant rise at 2 g/L [71]. PFOA degradation efficiencies are decreased from 98.2 % to 76 % with an increase in the graphene oxide- titanium dioxide anode for 4 h [65]. BiOI@Bi_5O_7I heterojunction electrodes increased the PFOA degradation rate from 30 % to 82 % (0.1 to 0.7 g/L), whereas the values diminished to around 70 and 50 % at 1.0 and 2.0 g/L. [76]. The corresponding decrease in defluorination/degradation values for higher loadings is due to the agglomeration of the catalyst and the scattering effect of the irradiated light.

5.3 Effect of pH

In general acidic environments (3 < pH < 5) are observed with better PFOA degradation, whereas extreme pH (< 2) is not suitable due to pKa (PFOA) ~ 2.8. A pH of 3.7 (without any adjustment) was observed with better PFOA defluorination for a pH range of 2.5 – 9.5 in the In_2O_3/persulfate system [60]. Similar behavior was observed for carbon aerogel with persulfate system where the corresponding defluorination and degradation values are reduced with an increase in the pH values where the kinetic rate constants (k_{ob}s) observed as 0.47 (pH 2), 0.33 (pH 3.8), 0.28 (pH 6.5), 0.22 (pH 11) [92]. Ga_2O_3/UV system assisted by peroxymonosulfate observed with better PFOA degradation (254 nm) parameters in pH 3 (100 %) over another pH 5/7/10 (86 %, 78 %, and 27 %) following the pseudo-first-order (PFO) kinetics [85]. Fe(TPFPP)/BC-PS-AA system reported better PFOA degradation at pH 2 over the wide window of experimental conditions (pH: 1, 2, 3, 5, 7, 9, 11) [71]. The corresponding degradation values are observed around 90.69 % and 49.02 % for pH 2, pH 11 conditions, respectively. Photo-electrochemical degradation of perfluorooctanoic acid (PFOA) with GOP25/FTO anodes reported with kinetic rate constants of 0.0074 min^{-1}, 0.0062 min^{-1}, and

0.0033 min^{-1} for pH 2, 5.3 and 10 respectively [65]. Fe/TNTs@AC showed no significant influence of pH over the range of 4 - 8, with an average defluorination of 61.3 % (4 h, UV irradiation) [66]. Whereas for pH 9, pH 10, and pH 11 conditions, the defluorination values dropped to 56.8 %, 42.7 %, and 36.1 %, respectively. BiOI@Bi_5O_7I heterojunction PFOA photocatalytic degradation was also reported with better parameters in pH 3 – 4.2, whereas the increase in the pH values inhibited the process [76]. In a recent study, the PFOS degradation was also observed with an influencing effect of pH, where Fe-Zeolites reported better photo-degradation in pH 3 over pH 5.5 and pH 7 [70]. PFOS exists in the anionic form in all environmental pH conditions (i.e., 2 - 14) due to its very low pK_a value (< 0); hence hydrophobic adsorption plays a major role over electrostatic attraction. Low PFOS photo-degradation at the higher pH values (i.e., 5.5, 7) is due to the decrease in the complexed PFOS (i.e., PFOS-Fe^{3+}) resulting in the altered ligand environment at metal centres (Fe-OH ligand exchange with Fe–H_2O). A similar mechanism was also reported for PFOA systems with a negative influence pH on degradation parameters onto Fe-zeolites with molecular oxygen as oxidant [69]. Low pH improves the H+ concentration hindering the production of •OH results in better PFOA decomposition efficiency in the PEC system. Whereas higher pH values result in hydroxyl ions (OH^-), which acts as a scavenger of sulfate radicals in retarding the PFOA decomposition. In addition, abundant OH^- ions in alkaline systems would react with •OH, further inhibiting the PFOA degradation process. Therefore, the corresponding values of PFOA decomposition are significant in acidic conditions over alkaline systems. In a recent study the modified coal combustion residuals-fly ash (FA-SCA) were also reported with a better PFASs removal in acidic conditions, in addition the influence of temperature and electrolytes onto PFAS removal abilities can be observed in **Figure 15** [108].

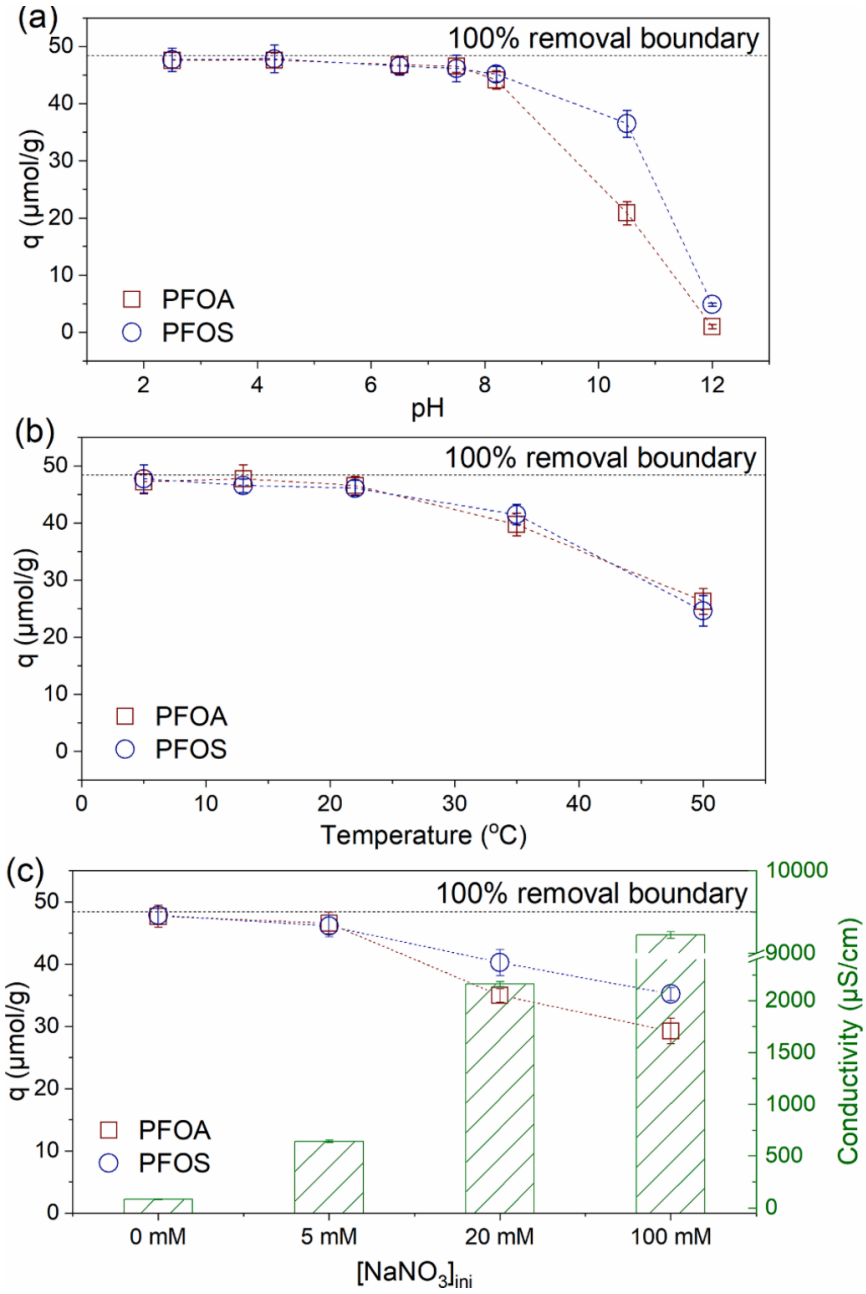

Figure 15. *The evaluation of water conditions (a) pH, (b) temperature, and (c) ionic strength on PFOX removal efficiency ([PFOX]ini = 1.21 μM, FA dose 25 mg/L, pH 7.5 and 22 ◦C in synthetic lake water if not particularly indicated).* [108] (Copyright Elsevier).

5.4 Radical species activity

The influence of the initial persulfate (PS) concentration and the amount of dissolved oxygen (DO) are major factors in delivering the high intense radical species (e.g., $SO_4^{\bullet -}$ and •OH) towards PFAS degradation. A decrement in the PFOA degradation efficiency was observed

for high PS concentrations (> 50 mM) with carbon aerogel, which may be due to the competence of high dense radical species resulting in self-scavenging (or) passivation of the remaining PS [92]. In the In_2O_3/persulfate system, the best PFOA defluorination performance was observed in 10 mM PS where low concentration failed to provide sufficient radicals. The synergistic effect between holes and radicals on defluorination ratio of PFOA using In_2O_3/PS under solar light irradiation are provided in **Figure 16** [60]**.**

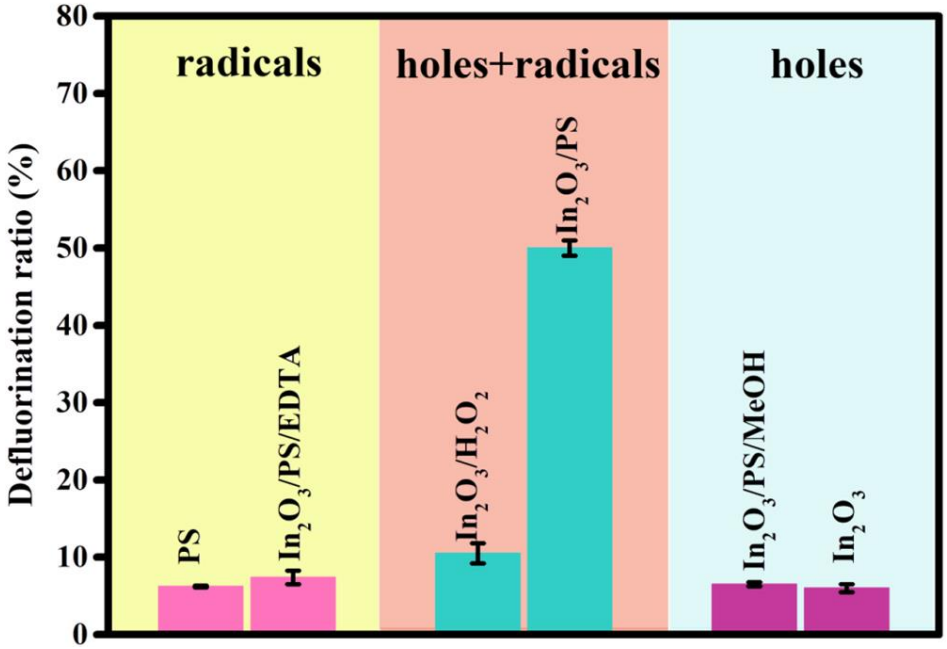

Figure 16. The synergistic effect between holes and radicals on defluorination ratio of PFOA in In_2O_3/PS system under solar light irradiation [60]. (Copyright Elsevier).

Decomposition of perfluorooctanoic acid by carbon aerogel (CA) with persulfate receives better values in low dosage levels (10 – 50 mM), whereas the higher doses (50 – 100 mM) resulted in no clear additional increase [92]. The possible occurrence of a large quantity of radicals ($SO_4^{\bullet -}$) in the CA+PS system could scavenge themselves or consume the remaining PS ($k \sim 4 \times 10^8\ M^{-1}s^{-1}$). The synergistic catalytic ability of CA resulted in dense radical species, whereas PFOA removal increased with the rise in the PS concentrations (10 to 100 mM) for the PS-only system (i.e., CA is absent). In iron-porphyrin loaded biochar

(Fe(TPFPP)/BC) catalyst different persulfate concentrations (0, 6.0, 12.1, 24.2, 36.2, 60.49 mM) were verified an the highest degradation values of 97.9 % are observed for 60.4 mM PS system [71]. An optimal PS quantity is necessary as radical-scavenging accelerates due to excessive SO_4^{-}• could react with $S_2O_8^{2-}$ and cause self-consumption at higher PS loadings.

5.5 Effect of Temperature and light source

An increase in operating temperature would improve most of the chemical reaction rates, but the possible application in wastewater treatment is a hurdle considering the energy efficiency aspects (**Figure 15b**). Better adsorption of PFOS/PFOA species onto various catalytic adsorbents in higher temperatures (endothermic reaction) would enhance the adsorption-assisted degradation reactions. Carbon aerogel with persulfate systems observed in the PFOA degradation and defluorination values increase from around 10 % to 85 % and 1 % to 35 %, respectively, for the temperature range of 25 – 60 ^{O}C [92]. At the same time, no significant influence of operating temperature was observed on PFOS degradation for Fe-Zeolites in the range of 25 – 80 ^{O}C ($k_{obs,\ PFOS}$ increased by 1.3 times) [70]. This may be due to them following the photon excitation efficiency of specific complexes (i.e., PFOS-Fe^{3+}) in the given temperature zone, limiting the photochemical degradation process. The effect of light sources on the efficacy and photo-degradation of PFOA was evaluated for peroxymonosulfate (PMS) assisted Ga_2O_3/UV system in UV light (185nm - 254 nm) and visible light (400 nm - 800 nm) bands [85]. UV light (~ 185 nm) has given higher degradation efficacy (100 %) of PFOA within 60 minutes, while 254nm UV source was observed for 120 min for complete degradation. Significant degradation values were not observed for visible band sources (400 – 800 nm). The corresponding reaction parameters were reported as PFOA: 50 mg L^{-1}, PMS: 1.23 g L^{-1}, Ga_2O_3: 0.25 g L^{-1}, and pH 3.

5.6 Effect of organic matter and other competing ions

A significant impact on the degradation and defluorination parameters in the presence of natural organic material (NOM) of 0.1 and 1 mg L^{-1} concentrations (SRFA or SRHA) was not observed [94]. The HFPO-TA degraded through the simultaneous aliphatic chain cleavage and stepwise defluorination processes. At the same time, a six-fold better presence of total organic compounds (TOC) with the Ceramic/PbO_2-PTFE anode with the conventional anode confirms the efficacy in the mineralization of the degraded organic compounds [90]. Better PFOS degradation was observed at low concentrations (89.0 ± 2.8%) to higher concentrations (76.4 ± 3.6%) for the air cathode-based EC process; this might be due to the formation of hemi-micelles by PFOS hindering the process [82]. PFOA degradation could be significantly inhibited by the presence of humic acid (HA) as it would be a competitor for radicals (e.g., $SO_4^{\bullet-}$) [92]. A comparative study on the effect of competing ions Cl^- and CO_3^{2-} on PFOA degradation was observed with better inhibition from the carbonate ions [71]. The differences in the redox potentials of the respective anion radicals (i.e., $Cl^{\cdot} > Cl_2^{-\cdot} > CO_3^{-\cdot}$) are observed to be the main reason for the inhibition activity. A significant inhibition effect was reported for PFOA degradation with sulfate ions (SO_4^{2-}) onto Fe-zeolites relative to other anions nitrate (NO_3^-), chloride (Cl^-), and perchlorate (ClO_4^-) [69]. The aspects of competitive complexation with metal centres and capture of hydroxyl radicals (•OH) are observed as the possible factors in the inhibition mechanism. In a few instances, the amount of dissolved oxygen (DO) also played a vital role in the PFAS degradation process. Molecular oxygen present in the aliquots synergizes the generation of radical species (•OH and $•O_2H$) and facilitates the redox reactions and corresponding radical complex chemistry. Thus the influence of NOM and other constituents have to be analyzed as they would cause significant variation in the DO values (**Figure 17**).

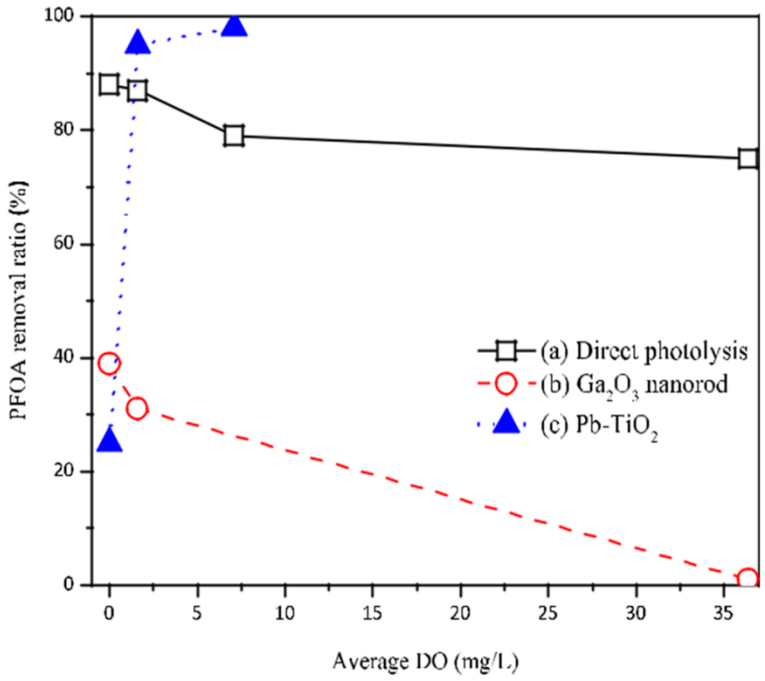

Figure 17. *Influence of DO on PFOA degradation by various photodecomposition methods*. [33] (Copyright Elsevier).

6. Future perspectives and Conclusions

Photo-Electrochemical technologies have shown to be promising for PFAS degradation, displaying better removal rates, capability for full mineralization, and economical regeneration of various catalyst/electrode materials based on electrochemical control. In the larger context of the photo-degradation abilities (Photo-oxidation and photo-reduction) of the PFAS substances the electrode materials have to be thoroughly analysed for the interaction abilities like electrostatic, hydrophobic, and π-anion etc. along with ligand and hydrogen–bond exchange reactions. In a similar grounds the wider working spectrum of the electrodes is highly in demand i.e., some may emphasize the degradation based on UV and Vis conditions. In the UV activated electrode materials there is a serious performance aspects among UVA, UVB, and etc. spectra. So the major applicability of these come into effect when they can have working ability in the Uv-Vis spectra where the Vis-spectra working aspects are highly appreciated. Hence the futuristic research and developmental have to be focussed in enhancing

the wider spectra applications of the novel electrode materials. In line of same interest the fate and transport behavior of the intermediate products (e.g., PFHpA: $C_6F_{13}COOH$) released during the degradation process.

The development of PFASs in the 1930's in some locations and their regular usage in water repellent surfaces and fire-retardant Film Forming Foam (FFF) in 40's, 50's and 60's over the globe has resulted in the present issue. Thus, the research perspective is evident in providing alarming conditions to the scientific community/peers to be practical and logical in proposing novel materials for larger-scale applications. Though there are site-specific (i.e., country-based) studies in calculating the ill-effects of the contamination, a total estimation of aspects and their direct/in-direct effects in the last few decades on the native of this land (i.e., all countries) is quite a difficult task.

As the intermediates are equally dangerous as same as the longer order products, and intermediates may proceed into various other reactions in resulting highly toxic compounds. The interdependence of the variables (e.g., pH, current density, potential, competing ions, and ROS) onto novel electrode materials need to be analysed to understand the degradation and synergistic mechanism at the microscopic level. In the last the energy aspects [i.e., Energy per order magnitude (EE/O)] need to be emphasized with utmost care and concern. As these novel materials will come into the larger scale applications (or) existence in fulfilling the condition of the cost-effectiveness as well as energy efficient. In addition to the regular PFASs (PFOS, PFAS), other similar products i.e., substitutes to conventional PFASs (e.g., GenX) should also to be verified with the electrode materials.

The present review discusses the various electrode (or) catalyst materials in different photocatalytic and photo-electrocatalytic degradation techniques for PFASs treatment. A vast class of electrode materials are detailed with a major focus onto PFOS and PFOA contaminant

species which are majorly long-chained PFASs. In the same intensity the detailed discussion onto smaller-chain PFASs are also need to be discussed. The energy aspects, repeatability, regeneration, cost-effectiveness, and utilization in complex conditions are a few challenging aspects in large-scale applications. These issues are to be discussed in a detailed manner alongside the environmental friendliness of each catalyst or hybrid-composite electrode towards developing efficient remediation cycles. In addition to the catalytic modules the synergistic themes supporting the degradation co-efficient (e.g., redox behavior and radical species generation) are also play a vital role (**Figure 18**). The fate and transport aspects of these contaminants and the catalyst electrodes have to be discussed for long-term aspects and sustainability approach.

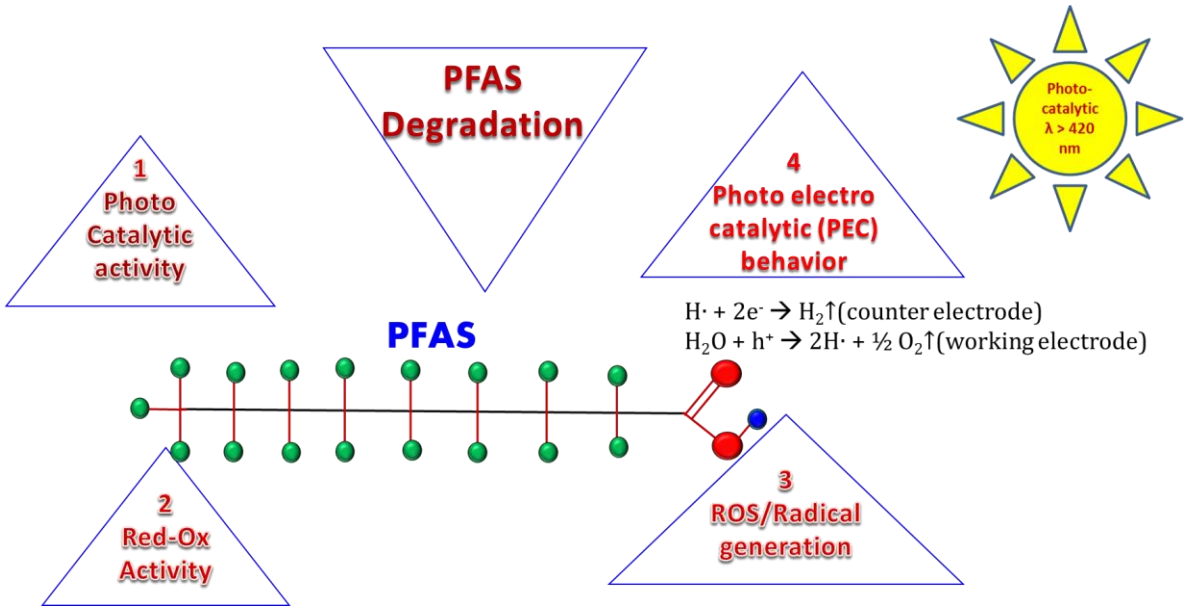

Figure 18. Schematic representation of the PFAS degradation aspects in Photo-catalytic/electrocatalytic and related modules.

Author Contributions:

Y. K. Penke: Conceptualization, Resources, Visualization, Writing Original Draft, Writing - Review & Editing. **K.K. Kar**: Writing - Review & Editing.

Notes: The author/s declare no known competing financial interests.

Acknowledgements:

YKP would like to thank Dr. Piyush Sharma (IIT-ISM, Dhanbad) and Dr. Ramesh Erelli (KITS, Warangal) for providing necessary assistance during the final corrections of this review article. Y.K.P would also like to thank "Elsevier Reviewers Hub" [i.e., Rewards section] for providing complimentary access to Scopus, Science Direct, and the corresponding Journals list, which provided assistance in procuring the state-of-the art literature.

References

[1] J. Aravind kumar, T. Krithiga, S. Sathish, A.A. Renita, D. Prabu, S. Lokesh, R. Geetha, S.K.R. Namasivayam, M. Sillanpaa, Persistent organic pollutants in water resources: Fate, occurrence, characterization and risk analysis, Sci. Total Environ. 831 (2022) 154808. doi:10.1016/j.scitotenv.2022.154808.

[2] L. Girones, A.L. Oliva, V.L. Negrin, J.E. Marcovecchio, A.H. Arias, Persistent organic pollutants (POPs) in coastal wetlands: A review of their occurrences, toxic effects, and biogeochemical cycling, Mar. Pollut. Bull. 172 (2021). doi:10.1016/j.marpolbul.2021.112864.

[3] Y. Vasseghian, S. Hosseinzadeh, A. Khataee, E.N. Dragoi, S. Adithya, R.S. Jayaraman, A. Krishnan, R. Malolan, K.P. Gopinath, J. Arun, W. Kim, M. Govarthanan, L. Girones, A.L. Oliva, V.L. Negrin, J.E. Marcovecchio, A.H. Arias, I. Sheriff, S.A. Debela, A. Mans-Davies, J. Aravind kumar, T. Krithiga, S. Sathish, A.A. Renita, D. Prabu, S. Lokesh, R. Geetha, S.K.R. Namasivayam, M. Sillanpaa, The concentration of persistent organic pollutants in water resources: A global systematic review, meta-analysis and probabilistic risk assessment, Sci. Total Environ. 271 (2021) 9–15. doi:10.1016/j.envsci.2022.01.005.

[4] A. Hirke, B. Varghese, S. Varade, R. Adela, Exposure to endocrine-disrupting chemicals and risk of gestational hypertension and preeclampsia: A systematic review and meta-analysis, Environ. Pollut. 317 (2023) 120828. doi:10.1016/j.envpol.2022.120828.

[5] Z. Yang, H. yu Liu, Q. yun Yang, X. Chen, W. Li, J. Leng, N. jun Tang, Associations between exposure to perfluoroalkyl substances and birth outcomes: A meta-analysis, Chemosphere. 291 (2022) 132909. doi:10.1016/j.chemosphere.2021.132909.

[6] S. Adithya, R.S. Jayaraman, A. Krishnan, R. Malolan, K.P. Gopinath, J. Arun, W. Kim, M. Govarthanan, A critical review on the formation, fate and degradation of the

persistent organic pollutant hexachlorocyclohexane in water systems and waste streams, Chemosphere. 271 (2021) 129866. doi:10.1016/j.chemosphere.2021.129866.

[7] I. Sheriff, S.A. Debela, A. Mans-Davies, The listing of new persistent organic pollutants in the stockholm convention: Its burden on developing countries, Environ. Sci. Policy. 130 (2022) 9–15. doi:10.1016/j.envsci.2022.01.005.

[8] M. Park, S. Wu, I.J. Lopez, J.Y. Chang, T. Karanfil, S.A. Snyder, Adsorption of perfluoroalkyl substances (PFAS) in groundwater by granular activated carbons: Roles of hydrophobicity of PFAS and carbon characteristics, Water Res. 170 (2020) 115364. doi:10.1016/j.watres.2019.115364.

[9] S.P. Lenka, M. Kah, L.P. Padhye, A review of the occurrence, transformation, and removal of poly- and perfluoroalkyl substances (PFAS) in wastewater treatment plants, Water Res. 199 (2021) 117187. doi:10.1016/j.watres.2021.117187.

[10] S. Kurwadkar, J. Dane, S.R. Kanel, M.N. Nadagouda, R.W. Cawdrey, B. Ambade, G.C. Struckhoff, R. Wilkin, Per- and polyfluoroalkyl substances in water and wastewater: A critical review of their global occurrence and distribution, Sci. Total Environ. (2021) 151003. doi:10.1016/j.scitotenv.2021.151003.

[11] I.M. Militao, F.A. Roddick, R. Bergamasco, L. Fan, Removing PFAS from aquatic systems using natural and renewable material-based adsorbents: A review, J. Environ. Chem. Eng. 9 (2021) 105271. doi:10.1016/j.jece.2021.105271.

[12] J. John, F. Coulon, P.V. Chellam, Detection and treatment strategies of per- and polyfluoroalkyl substances (PFAS): Fate of PFAS through DPSIR framework analysis, J. Water Process Eng. 45 (2022) 102463. doi:10.1016/j.jwpe.2021.102463.

[13] E. Gagliano, M. Sgroi, P.P. Falciglia, F.G.A. Vagliasindi, P. Roccaro, Removal of poly- and perfluoroalkyl substances (PFAS) from water by adsorption: Role of PFAS chain length, effect of organic matter and challenges in adsorbent regeneration, Water Res.

171 (2020) 115381. doi:10.1016/j.watres.2019.115381.

[14] M. Veciana, J. Bräunig, A. Farhat, M.L. Pype, S. Freguia, G. Carvalho, J. Keller, P. Ledezma, Electrochemical oxidation processes for PFAS removal from contaminated water and wastewater: fundamentals, gaps and opportunities towards practical implementation, J. Hazard. Mater. 434 (2022) 128886. doi:10.1016/j.jhazmat.2022.128886.

[15] H. Yu, H. Chen, B. Fang, H. Sun, Sorptive removal of per- and polyfluoroalkyl substances from aqueous solution: Enhanced sorption, challenges and perspectives, Sci. Total Environ. (2022) 160647. doi:10.1016/j.scitotenv.2022.160647.

[16] M. Wang, Y. Cai, B. Zhou, R. Yuan, Z. Chen, H. Chen, Removal of PFASs from water by carbon-based composite photocatalysis with adsorption and catalytic properties: A review, Sci. Total Environ. 836 (2022) 155652. doi:10.1016/j.scitotenv.2022.155652.

[17] K. Sivagami, P. Sharma, A. V Karim, G. Mohanakrishna, S. Karthika, G. Divyapriya, R. Saravanathamizhan, A.N. Kumar, Science of the Total Environment Electrochemical-based approaches for the treatment of forever chemicals : Removal of per fl uoroalkyl and poly fl uoroalkyl substances (PFAS) from wastewater, Sci. Total Environ. (2022) 160440. doi:10.1016/j.scitotenv.2022.160440.

[18] B. Xu, S. Liu, J.L. Zhou, C. Zheng, J. Weifeng, B. Chen, T. Zhang, W. Qiu, PFAS and their substitutes in groundwater: Occurrence, transformation and remediation, J. Hazard. Mater. 412 (2021) 125159. doi:10.1016/j.jhazmat.2021.125159.

[19] N. Bolan, B. Sarkar, M. Vithanage, G. Singh, D.C.W. Tsang, R. Mukhopadhyay, K. Ramadass, A. Vinu, Y. Sun, S. Ramanayaka, S.A. Hoang, Y. Yan, Y. Li, J. Rinklebe, H. Li, M.B. Kirkham, Distribution, behaviour, bioavailability and remediation of poly- and per-fluoroalkyl substances (PFAS) in solid biowastes and biowaste-treated soil, Environ. Int. 155 (2021) 106600. doi:10.1016/j.envint.2021.106600.

[20] S. Garg, P. Kumar, V. Mishra, R. Guijt, P. Singh, L.F. Dumée, R.S. Sharma, A review on the sources, occurrence and health risks of per-/poly-fluoroalkyl substances (PFAS) arising from the manufacture and disposal of electric and electronic products, J. Water Process Eng. 38 (2020) 101683. doi:10.1016/j.jwpe.2020.101683.

[21] A. Podder, A.H.M.A. Sadmani, D. Reinhart, N. Bin Chang, R. Goel, Per and poly-fluoroalkyl substances (PFAS) as a contaminant of emerging concern in surface water: A transboundary review of their occurrences and toxicity effects, J. Hazard. Mater. 419 (2021) 126361. doi:10.1016/j.jhazmat.2021.126361.

[22] A.F. Ojo, C. Peng, J.C. Ng, Assessing the human health risks of per- and polyfluoroalkyl substances: A need for greater focus on their interactions as mixtures, J. Hazard. Mater. 407 (2021) 124863. doi:10.1016/j.jhazmat.2020.124863.

[23] R. Dhore, G.S. Murthy, Per/polyfluoroalkyl substances production, applications and environmental impacts, Bioresour. Technol. 341 (2021) 125808. doi:10.1016/j.biortech.2021.125808.

[24] H.N. Phong Vo, H.H. Ngo, W. Guo, T.M. Hong Nguyen, J. Li, H. Liang, L. Deng, Z. Chen, T.A. Hang Nguyen, Poly-and perfluoroalkyl substances in water and wastewater: A comprehensive review from sources to remediation, J. Water Process Eng. 36 (2020) 101393. doi:10.1016/j.jwpe.2020.101393.

[25] W. Mei, H. Sun, M. Song, L. Jiang, Y. Li, W. Lu, G.G. Ying, C. Luo, G. Zhang, Per- and polyfluoroalkyl substances (PFASs) in the soil–plant system: Sorption, root uptake, and translocation, Environ. Int. 156 (2021) 106642. doi:10.1016/j.envint.2021.106642.

[26] D.Q. Zhang, W.L. Zhang, Y.N. Liang, Adsorption of perfluoroalkyl and polyfluoroalkyl substances (PFASs) from aqueous solution - A review, Sci. Total Environ. 694 (2019) 133606. doi:10.1016/j.scitotenv.2019.133606.

[27] R. Mukhopadhyay, B. Sarkar, K.N. Palansooriya, J.Y. Dar, N.S. Bolan, S.J. Parikh, C.

Sonne, Y.S. Ok, Natural and engineered clays and clay minerals for the removal of poly- and perfluoroalkyl substances from water: State-of-the-art and future perspectives, Adv. Colloid Interface Sci. 297 (2021) 102537. doi:10.1016/j.cis.2021.102537.

[28] T.H. Boyer, Y. Fang, A. Ellis, R. Dietz, Y.J. Choi, C.E. Schaefer, C.P. Higgins, T.J. Strathmann, Anion exchange resin removal of per- and polyfluoroalkyl substances (PFAS) from impacted water: A critical review, Water Res. 200 (2021) 117244. doi:10.1016/j.watres.2021.117244.

[29] F. Dixit, R. Dutta, B. Barbeau, P. Berube, M. Mohseni, PFAS removal by ion exchange resins: A review, Chemosphere. 272 (2021) 129777. doi:10.1016/j.chemosphere.2021.129777.

[30] M.A. Uriakhil, T. Sidnell, A. De Castro Fernández, J. Lee, I. Ross, M. Bussemaker, Per- and poly-fluoroalkyl substance remediation from soil and sorbents: A review of adsorption behaviour and ultrasonic treatment, Chemosphere. 282 (2021) 131025. doi:10.1016/j.chemosphere.2021.131025.

[31] D.M. Wanninayake, Comparison of currently available PFAS remediation technologies in water: A review, J. Environ. Manage. 283 (2021) 111977. doi:10.1016/j.jenvman.2021.111977.

[32] D. Leonello, M.A. Fendrich, F. Parrino, N. Patel, M. Orlandi, A. Miotello, Light-induced advanced oxidation processes as pfas remediation methods: A review, Appl. Sci. 11 (2021) 8458. doi:10.3390/app11188458.

[33] B. Xu, M.B. Ahmed, J.L. Zhou, A. Altaee, M. Wu, G. Xu, Photocatalytic removal of perfluoroalkyl substances from water and wastewater: Mechanism, kinetics and controlling factors, Chemosphere. 189 (2017) 717–729. doi:10.1016/j.chemosphere.2017.09.110.

[34] L. Yang, L. He, J. Xue, Y. Ma, Z. Xie, L. Wu, M. Huang, Z. Zhang, Persulfate-based

degradation of perfluorooctanoic acid (PFOA) and perfluorooctane sulfonate (PFOS) in aqueous solution: Review on influences, mechanisms and prospective, J. Hazard. Mater. 393 (2020) 122405. doi:10.1016/j.jhazmat.2020.122405.

[35] S. Wang, Q. Yang, F. Chen, J. Sun, K. Luo, F. Yao, X. Wang, D. Wang, X. Li, G. Zeng, Photocatalytic degradation of perfluorooctanoic acid and perfluorooctane sulfonate in water: A critical review, Chem. Eng. J. 328 (2017) 927–942. doi:10.1016/j.cej.2017.07.076.

[36] S. Sharma, N.P. Shetti, S. Basu, M.N. Nadagouda, T.M. Aminabhavi, Remediation of per- and polyfluoroalkyls (PFAS) via electrochemical methods, Chem. Eng. J. 430 (2022) 132895. doi:10.1016/j.cej.2021.132895.

[37] A. Román Santiago, P. Baldaguez Medina, X. Su, Electrochemical remediation of perfluoroalkyl substances from water, Electrochim. Acta. 403 (2022) 139635. doi:10.1016/j.electacta.2021.139635.

[38] S. Garg, J. Wang, P. Kumar, V. Mishra, H. Arafat, R.S. Sharma, L.F. Dumée, Remediation of water from per-/poly-fluoroalkyl substances (PFAS) - Challenges and perspectives, J. Environ. Chem. Eng. 9 (2021) 105784. doi:10.1016/j.jece.2021.105784.

[39] M.B. Ahmed, M.M. Alam, J.L. Zhou, B. Xu, M.A.H. Johir, A.K. Karmakar, M.S. Rahman, J. Hossen, A.T.M.K. Hasan, M.A. Moni, Advanced treatment technologies efficacies and mechanism of per- and poly-fluoroalkyl substances removal from water, Process Saf. Environ. Prot. 136 (2020) 1–14. doi:10.1016/j.psep.2020.01.005.

[40] O.C. Olatunde, A.T. Kuvarega, D.C. Onwudiwe, Photo enhanced degradation of contaminants of emerging concern in waste water, Emerg. Contam. 6 (2020) 283–302. doi:10.1016/j.emcon.2020.07.006.

[41] O.C. Olatunde, A.T. Kuvarega, D.C. Onwudiwe, Photo enhanced degradation of polyfluoroalkyl and perfluoroalkyl substances, Heliyon. 6 (2020) e05614.

doi:10.1016/j.heliyon.2020.e05614.

[42] D. Banks, B.M. Jun, J. Heo, N. Her, C.M. Park, Y. Yoon, Selected advanced water treatment technologies for perfluoroalkyl and polyfluoroalkyl substances: A review, Sep. Purif. Technol. 231 (2020) 115929. doi:10.1016/j.seppur.2019.115929.

[43] W. Zhang, D. Zhang, Y. Liang, Nanotechnology in remediation of water contaminated by poly- and perfluoroalkyl substances: A review, Environ. Pollut. 247 (2019) 266–276. doi:10.1016/j.envpol.2019.01.045.

[44] S. Verma, R.S. Varma, M.N. Nadagouda, Remediation and mineralization processes for per- and polyfluoroalkyl substances (PFAS) in water: A review, Sci. Total Environ. 794 (2021) 148987. doi:10.1016/j.scitotenv.2021.148987.

[45] D. Lu, S. Sha, J. Luo, Z. Huang, X. Zhang Jackie, Treatment train approaches for the remediation of per- and polyfluoroalkyl substances (PFAS): A critical review, J. Hazard. Mater. 386 (2020) 121963. doi:10.1016/j.jhazmat.2019.121963.

[46] B. Ji, P. Kang, T. Wei, Y. Zhao, Challenges of aqueous per- and polyfluoroalkyl substances (PFASs) and their foreseeable removal strategies, Chemosphere. 250 (2020) 126316. doi:10.1016/j.chemosphere.2020.126316.

[47] J. Cui, P. Gao, Y. Deng, Destruction of Per- A nd Polyfluoroalkyl Substances (PFAS) with Advanced Reduction Processes (ARPs): A Critical Review, Environ. Sci. Technol. 54 (2020) 3752–3766. doi:10.1021/acs.est.9b05565.

[48] R.A. Dickman, D.S. Aga, A review of recent studies on toxicity, sequestration, and degradation of per- and polyfluoroalkyl substances (PFAS), J. Hazard. Mater. 436 (2022) 129120. doi:10.1016/j.jhazmat.2022.129120.

[49] P. Roesch, C. Vogel, F.G. Simon, Reductive defluorination and mechanochemical decomposition of per-and polyfluoroalkyl substances (PFASs): From present knowledge to future remediation concepts, Int. J. Environ. Res. Public Health. 17 (2020) 1–22.

doi:10.3390/ijerph17197242.

[50] J.N. Kuhn, Y.O. Sokefun, Aqueous-Phase Photocatalytic Degradation of Emerging Forever Chemical Contaminants, ChemistrySelect. 6 (2021) 5225–5240. doi:10.1002/slct.202101650.

[51] A. Cordner, G. Goldenman, L.S. Birnbaum, P. Brown, M.F. Miller, R. Mueller, S. Patton, D.H. Salvatore, L. Trasande, The True Cost of PFAS and the Benefits of Acting Now, Environ. Sci. Technol. 55 (2021) 9630–9633. doi:10.1021/acs.est.1c03565.

[52] B. Cantoni, A. Turolla, J. Wellmitz, A.S. Ruhl, M. Antonelli, Perfluoroalkyl substances (PFAS) adsorption in drinking water by granular activated carbon: Influence of activated carbon and PFAS characteristics, Sci. Total Environ. 795 (2021) 148821. doi:10.1016/j.scitotenv.2021.148821.

[53] D. Jia, Q. Li, K. Hanna, G. Mailhot, M. Brigante, Efficient removal of estrogenic compounds in water by Mn III -activated peroxymonosulfate : Mechanisms and application in sewage treatment, Environ. Pollut. 288 (2021) 117728. doi:https://doi.org/10.1016/j.envpol.2021.117728.

[54] A. Gabet, H. Metivier, C. De Brauer, G. Mailhot, M. Brigante, Hydrogen peroxide and persulfate activation using UVA-UVB radiation : Degradation of estrogenic compounds and application in sewage treatment plant waters, J. Hazard. Mater. 405 (2021) 124693. doi:https://doi.org/10.1016/j.jhazmat.2020.124693.

[55] M. Al Amin, Z. Sobhani, Y. Liu, R. Dharmaraja, S. Chadalavada, R. Naidu, J.M. Chalker, C. Fang, Recent advances in the analysis of per- and polyfluoroalkyl substances (PFAS)—A review, Environ. Technol. Innov. 19 (2020) 100879. doi:10.1016/j.eti.2020.100879.

[56] K.L. Rodriguez, J.H. Hwang, A.R. Esfahani, A.H.M.A. Sadmani, W.H. Lee, Recent developments of PFAS-detecting sensors and future direction: A review,

Micromachines. 11 (2020) 667. doi:10.3390/mi11070667.

[57] R.F. Menger, E. Funk, C.S. Henry, T. Borch, Sensors for detecting per- and polyfluoroalkyl substances (PFAS): A critical review of development challenges, current sensors, and commercialization obstacles+++, Chem. Eng. J. 417 (2021) 129133. doi:10.1016/j.cej.2021.129133.

[58] S. Pilli, A.K. Pandey, V. Pandey, K. Pandey, T. Muddam, B.K. Thirunagari, S.T. Thota, S. Varjani, R.D. Tyagi, Detection and removal of poly and perfluoroalkyl polluting substances for sustainable environment, J. Environ. Manage. 297 (2021) 113336. doi:10.1016/j.jenvman.2021.113336.

[59] M.W. Sima, P.R. Jaffé, A critical review of modeling Poly- and Perfluoroalkyl Substances (PFAS) in the soil-water environment, Sci. Total Environ. 757 (2021) 143793. doi:10.1016/j.scitotenv.2020.143793.

[60] Y. Yuan, L. Feng, X. He, X. Liu, N. Xie, Z. Ai, L. Zhang, J. Gong, Efficient removal of PFOA with an In2O3/persulfate system under solar light via the combined process of surface radicals and photogenerated holes, J. Hazard. Mater. 423 (2022) 127176. doi:10.1016/j.jhazmat.2021.127176.

[61] L.H. Yang, W.J. Yang, S.H. Lv, T.T. Zhu, H.M. Adeel Sharif, C. Yang, J. Du, H. Lin, Is HFPO-DA (GenX) a suitable substitute for PFOA? A comprehensive degradation comparison of PFOA and GenX via electrooxidation, Environ. Res. 204 (2022) 111995. doi:10.1016/j.envres.2021.111995.

[62] Y. Wang, L. Li, Y. Wang, H. Shi, L. Wang, Q. Huang, Electrooxidation of perfluorooctanesulfonic acid on porous Magnéli phase titanium suboxide Anodes: Impact of porous structure and composition, Chem. Eng. J. 431 (2022) 133929. doi:10.1016/j.cej.2021.133929.

[63] C. Zhu, J. Xu, S. Song, J. Wang, Y. Li, R. Liu, Y. Shen, TiO2 quantum dots loaded

sulfonated graphene aerogel for effective adsorption-photocatalysis of PFOA, Sci. Total Environ. 698 (2020) 134275. doi:10.1016/j.scitotenv.2019.134275.

[64] M.J. Rivero, P. Ribao, B. Gomez-Ruiz, A. Urtiaga, I. Ortiz, Comparative performance of TiO2-rGO photocatalyst in the degradation of dichloroacetic and perfluorooctanoic acids, Sep. Purif. Technol. 240 (2020) 116637. doi:10.1016/j.seppur.2020.116637.

[65] J.S. Yang, W.W.P. Lai, S.C. Panchangam, A.Y.C. Lin, Photoelectrochemical degradation of perfluorooctanoic acid (PFOA) with GOP25/FTO anodes: Intermediates and reaction pathways, J. Hazard. Mater. 391 (2020) 122247. doi:10.1016/j.jhazmat.2020.122247.

[66] F. Li, Z. Wei, K. He, L. Blaney, X. Cheng, T. Xu, W. Liu, D. Zhao, A concentrate-and-destroy technique for degradation of perfluorooctanoic acid in water using a new adsorptive photocatalyst, Water Res. 185 (2020) 116219. doi:10.1016/j.watres.2020.116219.

[67] S. Verma, B. Mezgebe, E. Sahle-Demessie, M.N. Nadagouda, Photooxidative decomposition and defluorination of perfluorooctanoic acid (PFOA) using an innovative technology of UV–vis/ZnxCu1-xFe2O4/oxalic acid, Chemosphere. 280 (2021) 130660. doi:10.1016/j.chemosphere.2021.130660.

[68] T. Tran, L. Abrell, M.L. Brusseau, J. Chorover, Iron-activated persulfate oxidation degrades aqueous Perfluorooctanoic acid (PFOA) at ambient temperature, Chemosphere. 281 (2021) 130824. doi:10.1016/j.chemosphere.2021.130824.

[69] L. Qian, A. Georgi, R. Gonzalez-Olmos, F.D. Kopinke, Degradation of perfluorooctanoic acid adsorbed on Fe-zeolites with molecular oxygen as oxidant under UV-A irradiation, Appl. Catal. B Environ. 278 (2020) 119283. doi:10.1016/j.apcatb.2020.119283.

[70] L. Qian, F.D. Kopinke, A. Georgi, Photodegradation of Perfluorooctanesulfonic Acid

on Fe-Zeolites in Water, Environ. Sci. Technol. 55 (2021) 614–622. doi:10.1021/acs.est.0c04558.

[71] W. He, Y. Zhu, G. Zeng, Y. Zhang, Y. Wang, M. Zhang, H. Long, W. Tang, Efficient removal of perfluorooctanoic acid by persulfate advanced oxidative degradation: inherent roles of iron-porphyrin and persistent free radicals, Chem. Eng. J. 392 (2020) 123640. doi:10.1016/j.cej.2019.123640.

[72] Y.Y. Liu, C.J. Ptacek, R.J. Baldwin, J.M. Cooper, D.W. Blowes, Application of zero-valent iron coupled with biochar for removal of perfluoroalkyl carboxylic and sulfonic acids from water under ambient environmental conditions, Sci. Total Environ. 719 (2020) 137372. doi:10.1016/j.scitotenv.2020.137372.

[73] T. Xu, H. Ji, Y. Gu, T. Tong, Y. Xia, L. Zhang, D. Zhao, Enhanced adsorption and photocatalytic degradation of perfluorooctanoic acid in water using iron (hydr)oxides/carbon sphere composite, Chem. Eng. J. 388 (2020) 124230. doi:10.1016/j.cej.2020.124230.

[74] Y. Wu, Y. Hu, M. Han, Y. Ouyang, L. Xia, X. Huang, Z. Hu, C. Li, Mechanism insights into the facet-dependent photocatalytic degradation of perfluorooctanoic acid on BiOCl nanosheets, Chem. Eng. J. 425 (2021) 130672. doi:10.1016/j.cej.2021.130672.

[75] T. Li, C. Wang, T. Wang, L. Zhu, Highly efficient photocatalytic degradation toward perfluorooctanoic acid by bromine doped BiOI with high exposure of (001) facet, Appl. Catal. B Environ. 268 (2020) 118442. doi:10.1016/j.apcatb.2019.118442.

[76] J. Wang, C. Cao, Y. Wang, Y. Wang, B. Sun, L. Zhu, In situ preparation of p-n BiOI@Bi5O7I heterojunction for enhanced PFOA photocatalytic degradation under simulated solar light irradiation, Chem. Eng. J. 391 (2020) 123530. doi:10.1016/j.cej.2019.123530.

[77] Z. Li, S. Li, Y. Tang, X. Li, J. Wang, L. Li, Highly efficient degradation of

perfluorooctanoic acid: An integrated photo-electrocatalytic ozonation and mechanism study, Chem. Eng. J. 391 (2020) 123533. doi:10.1016/j.cej.2019.123533.

[78] Z. Song, X. Dong, J. Fang, C. Xiong, N. Wang, X. Tang, Improved photocatalytic degradation of perfluorooctanoic acid on oxygen vacancies-tunable bismuth oxychloride nanosheets prepared by a facile hydrolysis, J. Hazard. Mater. 377 (2019) 371–380. doi:10.1016/j.jhazmat.2019.05.084.

[79] X. Liu, X. Duan, T. Bao, D. Hao, Z. Chen, W. Wei, D. Wang, S. Wang, B.J. Ni, High-performance photocatalytic decomposition of PFOA by BiOX/TiO2 heterojunctions: Self-induced inner electric fields and band alignment, J. Hazard. Mater. 430 (2022) 128195. doi:10.1016/j.jhazmat.2021.128195.

[80] Y.F. Li, C.Y. Hu, Y.C. Lee, S.L. Lo, Effects of zinc salt addition on perfluorooctanoic acid (PFOA) removal by electrocoagulation with aluminum electrodes, Chemosphere. 288 (2022) 132665. doi:10.1016/j.chemosphere.2021.132665.

[81] H. Shi, S.Y. (Dora) Chiang, Y. Wang, Y. Wang, S. Liang, J. Zhou, R. Fontanez, S. Gao, Q. Huang, An electrocoagulation and electrooxidation treatment train to remove and degrade per- and polyfluoroalkyl substances in aqueous solution, Sci. Total Environ. 788 (2021) 147723. doi:10.1016/j.scitotenv.2021.147723.

[82] T. Mu, M. Park, K.Y. Kim, Energy-efficient removal of PFOA and PFOS in water using electrocoagulation with an air-cathode, Chemosphere. 281 (2021) 130956. doi:10.1016/j.chemosphere.2021.130956.

[83] W. Zhang, H. Efstathiadis, L. Li, Y. Liang, Environmental factors affecting degradation of perfluorooctanoic acid (PFOA) by In2O3 nanoparticles, J. Environ. Sci. (China). 93 (2020) 48–56. doi:10.1016/j.jes.2020.02.028.

[84] S. Li, M. Gu, J. Huang, Y. Wang, G. Yu, Oligolayered Co@MXene with a Co···SO3 cation-π bridge for ultra-rapid catalytic oxidation of a novel “forever chemical” OBS,

Appl. Catal. B Environ. 311 (2022) 121364. doi:10.1016/j.apcatb.2022.121364.

[85] B. Xu, J.L. Zhou, A. Altaee, M.B. Ahmed, M.A.H. Johir, J. Ren, X. Li, Improved photocatalysis of perfluorooctanoic acid in water and wastewater by Ga2O3/UV system assisted by peroxymonosulfate, Chemosphere. 239 (2020) 124722. doi:10.1016/j.chemosphere.2019.124722.

[86] J. Zhu, Y. Chen, Y. Gu, H. Ma, M. Hu, X. Gao, T. Liu, Feasibility study on the electrochemical reductive decomposition of PFOA by a Rh/Ni cathode, J. Hazard. Mater. 422 (2022) 126953. doi:10.1016/j.jhazmat.2021.126953.

[87] H. Olvera-Vargas, Z. Wang, J. Xu, O. Lefebvre, Synergistic degradation of GenX (hexafluoropropylene oxide dimer acid) by pairing graphene-coated Ni-foam and boron doped diamond electrodes, Chem. Eng. J. 430 (2022) 132686. doi:10.1016/j.cej.2021.132686.

[88] L. Duan, B. Wang, K. Heck, S. Guo, C.A. Clark, J. Arredondo, M. Wang, T.P. Senftle, P. Westerhoff, X. Wen, Y. Song, M.S. Wong, Efficient Photocatalytic PFOA Degradation over Boron Nitride, Environ. Sci. Technol. Lett. 7 (2020) 613–619. doi:10.1021/acs.estlett.0c00434.

[89] J. Xie, C. Zhang, T. David Waite, Integrated flow anodic oxidation and ultrafiltration system for continuous defluorination of perfluorooctanoic acid (PFOA), Water Res. 216 (2022) 118319. doi:10.1016/j.watres.2022.118319.

[90] Z. Lou, J. Wang, S. Wang, Y. Xu, J. Wang, B. Liu, C. Yu, J. Yu, Strong hydrophobic affinity and enhanced •OH generation boost energy-efficient electrochemical destruction of perfluorooctanoic acid on robust ceramic/PbO2-PTFE anode, Sep. Purif. Technol. 280 (2022) 119919. doi:10.1016/j.seppur.2021.119919.

[91] M.S. Samuel, M. Shang, J. Niu, Photocatalytic degradation of perfluoroalkyl substances in water by using a duo-functional tri-metallic-oxide hybrid catalyst, Chemosphere. 293

(2022) 133568. doi:10.1016/j.chemosphere.2022.133568.

[92] Y.C. Lee, Y.F. Li, S.L. Lo, J. Kuo, W. Sun, C.Y. Hu, Decomposition of perfluorooctanic acid by carbon aerogel with persulfate, Chem. Eng. J. 430 (2022) 132900. doi:10.1016/j.cej.2021.132900.

[93] T. Xu, Y. Zhu, J. Duan, Y. Xia, T. Tong, L. Zhang, D. Zhao, Enhanced photocatalytic degradation of perfluorooctanoic acid using carbon-modified bismuth phosphate composite: Effectiveness, material synergy and roles of carbon, Chem. Eng. J. 395 (2020) 124991. doi:10.1016/j.cej.2020.124991.

[94] Z. Chen, Y. Teng, L. Huang, N. Mi, C. Li, J. Ling, C. Gu, X. Jin, Rapid photo-reductive destruction of hexafluoropropylene oxide trimer acid (HFPO-TA) by a stable self-assembled micelle system of producing hydrated electrons, Chem. Eng. J. 420 (2021) 130436. doi:10.1016/j.cej.2021.130436.

[95] A. Kugler, H. Dong, C. Li, C. Gu, C.E. Schaefer, Y.J. Choi, D. Tran, M. Spraul, C.P. Higgins, Reductive defluorination of Perfluorooctanesulfonic acid (PFOS) by hydrated electrons generated upon UV irradiation of 3-Indole-acetic-acid in 12-Aminolauric-Modified montmorillonite, Water Res. 200 (2021) 117221. doi:10.1016/j.watres.2021.117221.

[96] J.-M. Arana Juve, F. Li, Y. Zhu, W. Liu, L.D.M. Ottosen, D. Zhao, Z. Wei, Concentrate and degrade PFOA with a photo-regenerable composite of In-doped TNTs@AC, Chemosphere. 300 (2022) 134495. doi:10.1016/j.chemosphere.2022.134495.

[97] J. Hou, G. Li, M. Liu, L. Chen, Y. Yao, P.H. Fallgren, S. Jin, Electrochemical destruction and mobilization of perfluorooctanoic acid (PFOA) and perfluorooctane sulfonate (PFOS) in saturated soil, Chemosphere. 287 (2022) 132205. doi:10.1016/j.chemosphere.2021.132205.

[98] S. Tian, T. Xu, L. Fang, Y. Zhu, F. Li, R.N. Leary, M. Zhang, D. Zhao, T.Y. Soong, H.

Shi, A ‘Concentrate-&-Destroy’ technology for enhanced removal and destruction of per- and polyfluoroalkyl substances in municipal landfill leachate ++++, Sci. Total Environ. 791 (2021) 148124. doi:10.1016/j.scitotenv.2021.148124.

[99] G. Niarchos, M. Sörengård, F. Fagerlund, L. Ahrens, Electrokinetic remediation for removal of per- and polyfluoroalkyl substances (PFASs) from contaminated soil, Chemosphere. (2021) 133041. doi:10.1016/j.chemosphere.2021.133041.

[100] H. McIntyre, V. Minda, E. Hawley, R. Deeb, M. Hart, Coupled photocatalytic alkaline media as a destructive technology for per- and polyfluoroalkyl substances in aqueous film-forming foam impacted stormwater, Chemosphere. (2021) 132790. doi:10.1016/j.chemosphere.2021.132790.

[101] C.J. Liu, G. McKay, D. Jiang, R. Tenorio, J.T. Cath, C. Amador, C.C. Murray, J.B. Brown, H.B. Wright, C. Schaefer, C.P. Higgins, C. Bellona, T.J. Strathmann, Pilot-scale field demonstration of a hybrid nanofiltration and UV-sulfite treatment train for groundwater contaminated by per- and polyfluoroalkyl substances (PFASs), Water Res. 205 (2021) 117677. doi:10.1016/j.watres.2021.117677.

[102] J. Radjenovic, N. Duinslaeger, S.S. Avval, B.P. Chaplin, Facing the Challenge of Poly- And Perfluoroalkyl Substances in Water: Is Electrochemical Oxidation the Answer?, Environ. Sci. Technol. 54 (2020) 14815–14829. doi:10.1021/acs.est.0c06212.

[103] M.J. Bentel, Z. Liu, Y. Yu, J. Gao, Y. Men, J. Liu, Enhanced Degradation of Perfluorocarboxylic Acids (PFCAs) by UV/Sulfite Treatment: Reaction Mechanisms and System Efficiencies at pH 12, Environ. Sci. Technol. Lett. 7 (2020) 351–357. doi:10.1021/acs.estlett.0c00236.

[104] N. Duinslaeger, J. Radjenovic, Electrochemical degradation of per- and polyfluoroalkyl substances (PFAS) using low-cost graphene sponge electrodes, Water Res. 213 (2022) 118148. doi:10.1016/j.watres.2022.118148.

[105] H. Cao, W. Zhang, C. Wang, Y. Liang, H. Sun, Photodegradation of F–53B in aqueous solutions through an UV/Iodide system, Chemosphere. 292 (2022) 133436. doi:10.1016/j.chemosphere.2021.133436.

[106] J. Bao, W.J. Yu, Y. Liu, X. Wang, Z.Q. Liu, Y.F. Duan, Removal of perfluoroalkanesulfonic acids (PFSAs) from synthetic and natural groundwater by electrocoagulation, Chemosphere. 248 (2020) 125951. doi:10.1016/j.chemosphere.2020.125951.

[107] A.B. Nienhauser, M.S. Ersan, Z. Lin, F. Perreault, P. Westerhoff, S. Garcia-Segura, Boron-doped diamond electrodes degrade short- and long-chain per- and polyfluorinated alkyl substances in real industrial wastewaters, J. Environ. Chem. Eng. 10 (2022) 107192. doi:10.1016/j.jece.2022.107192.

[108] H. Wan, R. Mills, K. Qu, J.C. Hower, M.A. Mottaleb, D. Bhattacharyya, Z. Xu, Rapid removal of PFOA and PFOS via modified industrial solid waste: Mechanisms and influences of water matrices, Chem. Eng. J. 433 (2021) 133271. doi:10.1016/j.cej.2021.133271.